

杂原子掺杂闪光石墨烯支持信息 Heteroatom-Doped Flash Graphene—Supporting Information

陈伟音 , 1#张歌 , 1,2#李天慈 , 1,3雅各布 L 贝克汉姆 , 1哲元 , 1凯文 M 怀斯 , 1保罗 A 阿文丘拉 , 1
Weiyan Chen,^{1#} Chang Ge,^{1,2#} John Tianci Li,^{1,3} Jacob L. Beckham,¹ Zhe Yuan,¹ Kevin M. Wyss,¹

卢卡斯 艾迪 , 1,2卡特 基特雷尔 , 1陈金杭 , 1杜宣良 , 1罗伯特 A。
Paul A. Advincula,¹ Lucas Eddy,^{1,2} Carter Kittle, ¹ Jinhang Chen,¹ Duy Xuan Luong,¹ Robert A.

Carter,¹ James M. Tour^{1,3,4,5*}

化学系 , 2应用物理项目 , 3材料科学与工程系

¹Department of Chemistry, ²Applied Physics Program, ³Department of Materials Science and

美国德克萨斯州休斯顿大街6100号莱斯大学计算机科学系 , 纳米工程 , ⁴斯莫利旋涡研究所 , 纳米碳中心和韦
NanoEngineering, ⁴Smalley-Curl Institute, the NanoCarbon Center, and The Welch Institute for

尔奇先进材料研究所 , ⁵

Advanced Materials, and ⁵Department of Computer Science, Rice University, 6100 Main Street,

Houston, Texas 77005, United States

通讯作者(电子邮件 : tour@rice.edu)

*Corresponding Author (Email: tour@rice.edu)

这些作者对这项工作做出了同等贡献。

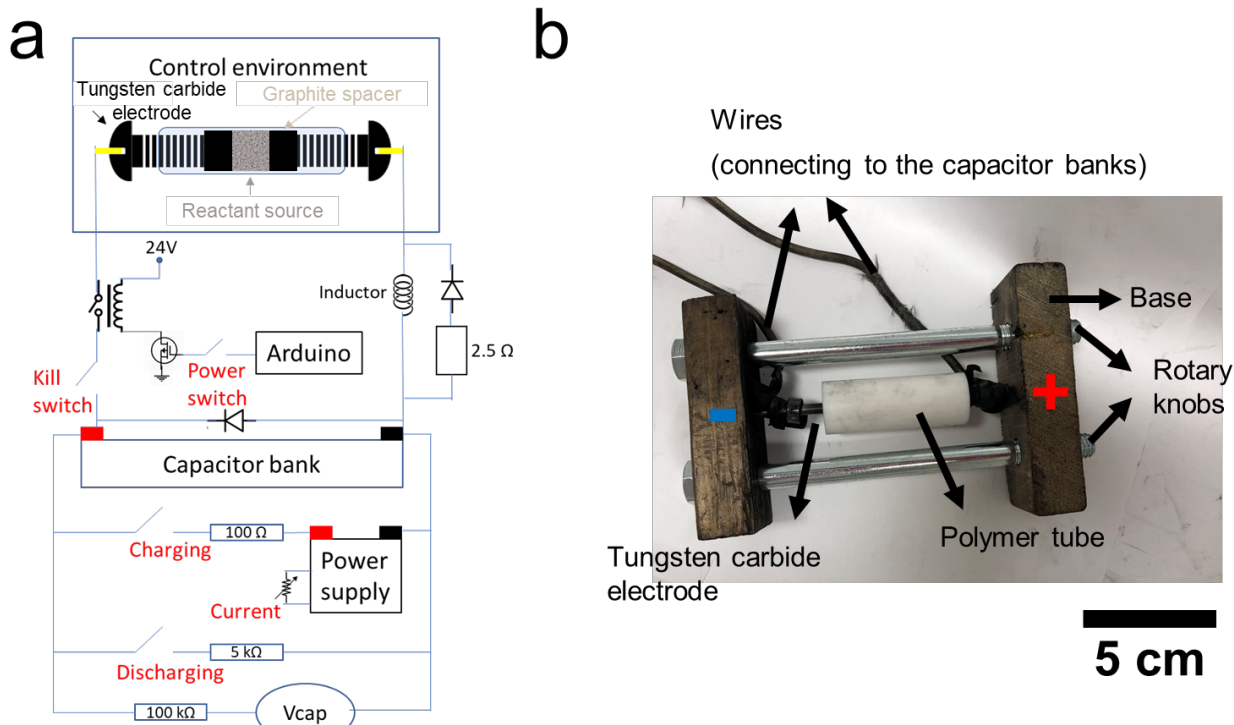
#These authors contributed equally to this work.

缩写

Abbreviations

B-FG掺硼闪光石墨烯	
B-FG	Boron doped flash graphene
B, N-FG硼氮共掺杂闪光石墨烯	
B,N-FG	Boron and nitrogen co-doped flash graphene
B, N , S-FG硼、氮和硫共掺杂闪光石墨烯	
B,N,S-FG	Boron, nitrogen and sulfur co-doped flash graphene
CG商用石墨烯纳米片	
CG	Commercial graphene nanoplatelets
F-FG掺氟闪光石墨烯	
F-FG	Fluorine doped flash graphene
FG闪光石墨烯	
FG	Flash graphene
FJH闪光焦耳加热	
FJH	Flash Joule heating
N-FG掺氮闪光石墨烯	
N-FG	Nitrogen doped flash graphene
O-FG氧掺杂闪光石墨烯	
O-FG	Oxygen doped flash graphene
P-FG掺磷闪光石墨烯	
P-FG	Phosphorous doped flash graphene
S-FG硫掺杂闪光石墨烯	
S-FG	Sulfur doped flash graphene
VFD变频驱动	
VFD	Variable frequency drive

闪光焦耳加热设置 Flash Joule Heating Setup



图S1。 (a) FJH设置的电路图。
Figure S1. (a) The circuit diagram of the FJH setup. The circuit diagram is adapted from our previous publication.¹⁻³ (b) FJH反应堆箱的光学照片。
Figure S1. (b) The optical photograph of the FJH reactor box.

FJH设置的电路图如图S1a所示。
The circuit diagram of the FJH setup is shown in Figure S1a. The electrical energy discharged through samples放电的电能来自电容器组，电容器组的总电容为 $60\sim222\text{ mF}$ ，具体取决于反应物的质量(有关更多详细信息，请参阅实验部分)。
through the sample is from the capacitor bank, which has a total capacitance of $60\sim222\text{ mF}$ depending on the reactant mass (See the Experimental Section for more details). The capacitor bank is charged by a dc. power supply that could reach 400 V. An Arduino controller relay with programmable millisecond-level delay time is used to control the discharge time, and the electric energy is provided by the capacitor bank. Safety glasses designed for welding are generally suitable and recommended during the flash reaction because they effectively block infrared as well as ultraviolet light. More safety notes follow below. The home-made FJH reaction box is

通过样品放电的电能来自电容器组，电容器组由直流电源充电。可达到400 V的电源。使用具有可编程毫秒级延迟时间的Arduino控制器继电器来控制放电时间，电能由电容器组提供。

设计用于焊接的安全眼镜通常适用于并推荐在闪光反应期间使用，因为它们可以有效阻挡红外线和紫外线。

更多安全注意事项如下。

国产FJH反应箱为

由一个木制底座、两个旋转旋钮和两个碳化钨电极组成，通过导线连接到电容器组。
composed of a wooden base, two rotary knobs and two tungsten carbide electrodes connected
with wires to the capacitor banks. The applied force can be adjusted by the rotary knob. The
施加的力可以通过旋钮进行调整。
carbonized
with wires to the capacitor banks. The applied force can be adjusted by the rotary knob. The
钨电极对样品的压缩越紧密，系统在闪速反应期间可以达到的电阻率越低。
tighter the tungsten carbide electrodes compress the sample, the lower resistivity the system can
在机器车间制备厚壁聚合物管 (ID=4 mm, OD=25 mm, 长度=6 cm),
reach during the flash reaction. The polymer tubes with thick wall (ID = 4 mm, OD = 25 mm,
例如聚四氟乙烯(PTFE)管、聚苯硫醚(PPS)管或聚丙烯腈(PAN)管，并用于容纳反应物。
length = 6 cm), such as polytetrafluoroethylene (PTFE) tube, poly(1,4-phenylene sulfide) (PPS)
tube or polyacrylonitrile (PAN) tubes are prepared in the machine shop and used to hold the
将制备好的粉末样品放置在直接接触碳化钨电极的两个石墨垫片之间。
reactants. The prepared powder sample is placed between the two graphite spacers that directly
contact the tungsten carbide electrodes. The reactants are compressed until the desired resistance
压缩反应物，直到达到所需电阻(1.0~5.0)。
闪光参数在实验部分和表1中描述。
(1.0~5.0 Ω) is reached. The flash parameters are described in the Experimental Section and
Table 1.

安全注意事项1-3 SAFETY NOTES¹⁻³

闪光焦耳加热(FJH)涉及高电流和高电压，有触电甚至触电的风险，因此应实施这些功能。
Flash Joule heating (FJH) involves high currents and voltages, which has a risk of
该列表并不全
electrical shock or even electrocution, so these features should be implemented. This list is
面，但说明了最小化风险所需的协议。
not intended to be comprehensive, but demonstrative of the protocols needed to minimize
risk.

1、封闭或小心绝缘所有接线。

1. Enclose or carefully insulate all wire connections.

所有连接、导线和部件必须适用于高电压和高电流。

2. All connections, wires and components must be suitable for the high voltages and
currents.

3、请注意，元件故障可能会导致高压出现在意外的地方，例如开关晶体管上的散热器。

3. Be aware that component failure could cause high voltage to appear in unexpected places,
such as heat sinks on the switching transistors.

4. 控制线应具有额定高压的光隔离器。

4. Control wires should have opto-isolators rated for high voltage.

- 5、提供一个可见的充电指示灯。** 230 V透明玻璃白炽灯泡是一个不错的选择，因为灯丝上的辉光还提供了电容器组上电荷量的近似指示器。
5. Provide a visible charge indicator. A 230 V clear glass incandescent light bulb is a good choice as the glow on the filament also provides an approximate indicator of the amount of charge on the capacitor bank. Bright light = danger!
强光=危险！
- 不要使用带有金属开关的拨动开关。** 如果产生电弧，金属开关可能带电。
6. Do not use toggle switches with metal toggles. If an arc develops, the metal toggle could become charged. Use only circuit breakers.
- 单手定则。** 在系统上工作时，只需一只手，另一只手不要接触任何接地表面。
7. One hand rule. Use only one hand when working on the system, with the other hand not touching any grounded surface.
- 8.在每个电容器上安装100000欧姆范围内的放电电阻器，使电荷在约1小时内始终放电。**
8. Install bleed resistors in the range of 100,000 ohms on each capacitor so that charge will always bleed off in ~1 h.
- 提供一个机械放电断路器开关，该开关连接到几百欧姆的功率电阻器，以快速释放电容器电荷。**
9. Provide a mechanical discharge circuit breaker switch connected to a power resistor of a few hundred ohms to rapidly bleed off the capacitor charge.
- 10.提供一个“关断”断路器开关，以断开样品架与电容器组的连接。**
10. Provide a "kill" circuit breaker switch to disconnect the sample holder from the capacitor bank.
- 11、提供交流隔离断路器开关。**
11. Provide an AC disconnect circuit breaker switch.
- 12、在设备上张贴高压警告标志。**
12. Post a high voltage warning signs on the apparatus.
- 使用断路器作为开关。** 断路器具有内置消弧功能，可中断1000安培或更大电流。
13. Use of circuit breakers as switches. Circuit breakers have built-in arc suppression that can interrupt 1000 amps or more. Conventional switches do not have such a high level of arc suppression and can burn out or weld closed due to the high current pulses.
- 14、使用额定直流电压的断路器。** 大多数交流断路器的直流额定值为电压的1/2或更低，因为直流电弧更难抑制。
14. Use circuit breakers rated for DC voltage. Most AC circuit breakers have a DC rating 1/2 the voltage or less, since DC arcs are much more difficult to suppress. Circuit breakers designed for DC solar power systems are a good choice.
- 选择断路器时，根据0.1 s的典型时间曲线进行选择，而不是稳态额定电流。**
15. When choosing circuit breakers, choose by the time curves typical for 0.1 s, rather than the steady state current rating. K-type DC circuit breakers will have ~10× higher trip
- K型直流断路器将具有约10×更高的跳闸

与额定电流相比，0.1秒时的电流，Z型断路器在0.1秒时将具有约 $4\times$ 更高的跳闸电流。
current at 0.1 s compared to their rated current, and Z-type breakers will have $\sim 4\times$ higher
大多数断路器中设计的这种“延迟跳闸”将允许比断路器静态额定值高得多的
trip current at 0.1 s. This "delayed trip" designed into most circuit breakers will allow
脉冲电流。
much higher pulse currents than the steady state rating of the breaker.

在放电电路中加入少量电感，以将上升时间限制在毫秒或更高。

16. Include a small amount of inductance in the discharge circuit to limit the rise time to a
极快的放电会损坏部件，并导致射频干扰其他实验室设备。
millisecond or more. Extremely fast discharges can damage components and cause RF
interference with other lab apparatus.

17. 请记住，系统可以在毫秒内放电数千焦耳，这可能导致继电器甚至电容器等部件爆炸。

17. Keep in mind that the system can discharge many thousands of Joules in milliseconds,
这些部
which can cause components such as relays or even capacitors to explode. These
件应封闭起来，以防止高压和可能的飞屑。
components should be enclosed to protect against both high voltage and possible flying
debris.

随时准备一个带有高压测试引线的电压表。

18. Keep a voltmeter with high voltage test leads handy at all times. When working on the
在电容器组上工作时，始
终检查每个电容器组上的电压。
capacitor bank, always check the voltage on each. A broken wire or loose connection
° could leave the capacitor in a charged state.

19. 使用仪器时，戴上延伸至肘部的厚橡胶手套，以防触电。

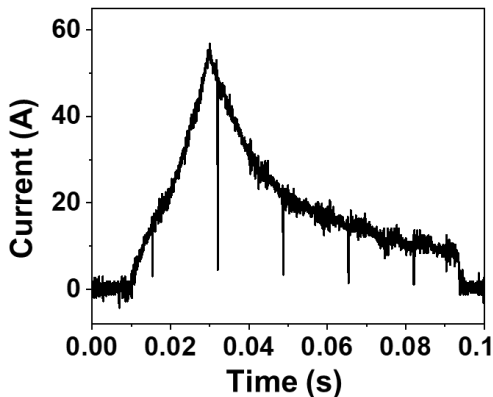
19. Wear thick rubber gloves extending to the elbows when using the apparatus to protect
from electrocution.

所有用户均应由经验丰富的电气技术人员进行适当培训。

20. All users should be properly trained by an experienced electrical technician.

21. 让合格的电气工程师在使用前检查仪器的安全性，并每周重新检查一次。

21. Have a qualified electrical engineer inspect the instrument for safety before its use and
have it reinspected weekly.



图S2。FJH合成过程中的电流-时间曲线。

Figure S2. Current-time curve during the FJH synthesis process.

电能总量可通过以下等式1计算。

The total amount of electrical energy can be calculated by eq 1 below.

$$E_i = \sum 0.5 \times C_{total} \times (V_1^2 - V_2^2) \quad (1)$$

对于N-FG，电压输入V1为110 V，总容量Ctotal为60 mF。

For N-FG, the voltage input V_1 is 110 V and the total capacity C_{total} is 60 mF. The flash repetition is 1. Therefore, the input electrical energy E_i is 265 J.

闪光重复次

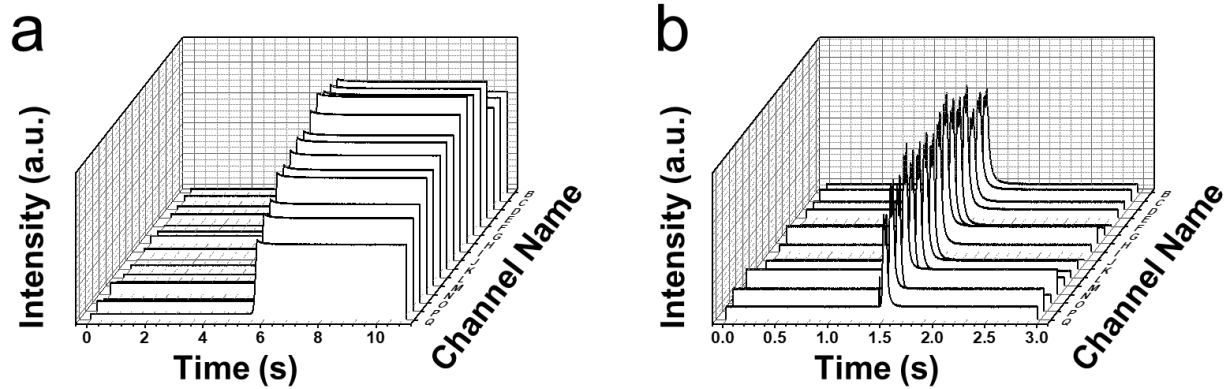
每克E反应物吸收的能量如等式2所示。

The energy that reactant absorbs per gram E is as in eq 2.

$$E = E_i/m \quad (2)$$

Since the mass m for each batch in this condition is 40 mg, E is 6.6 kJ g⁻¹, which converts to 1840 kWh per ton. Considering the electricity price is 2 cents per kWh (West Texas industrial rate), the energy cost is ~36.8 dollars per ton of sample. The total amount of electrical energy for different heteroatom-doped FG is listed in Table S1 below.

下表S1列出了不同掺杂杂原子FG的总电能。



图S3。用16通道光纤自制光谱仪记录的光谱。

Figure S3. The spectra recorded by the home-built spectrometer with 16-channel optical fibers.

(a) 2800 K时的标准参考。

(a) Standard reference at 2800 K. (b) The reaction temperature during the flash process. The

通道的波长范围为1000 nm至640 nm，间隔24 nm。

wavelengths of these channels range from 1000 nm to 640 nm at equal intervals of 24 nm.

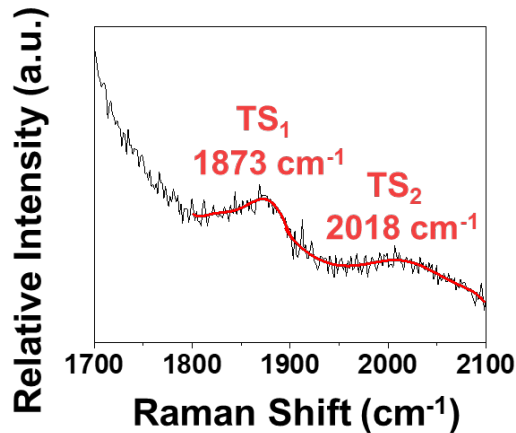
随后使用黑体辐射(BBR)拟合来获得每个时间点的温度，如图1b所示。

Blackbody radiation (BBR) fitting is subsequently used to obtain the temperature at each time

point as shown in Figure 1b.

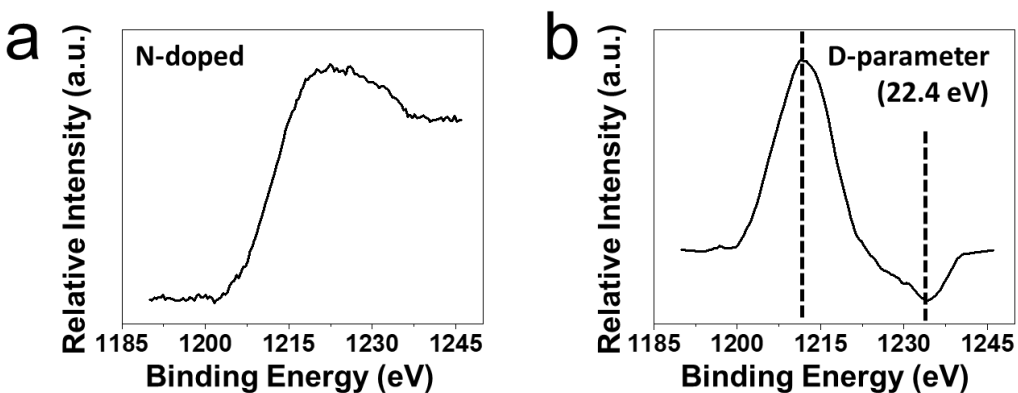
氮掺杂闪光石墨烯的表征

Characterization of nitrogen-doped flash graphene

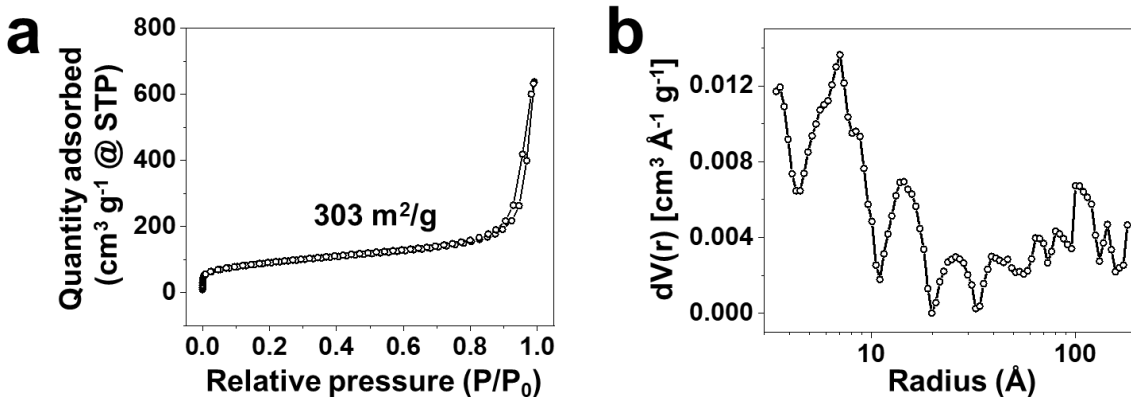


图S4。N-FG的高分辨率拉曼光谱证明了涡轮层结构的存在。

Figure S4. The high-resolution Raman spectrum of N-FG demonstrating the existence of turbostratic structure. In the spectrum, the TS₁ (~1873 cm⁻¹) and TS₂ (~2018 cm⁻¹) peaks can be distinguished, which are indicators for the presence of turbostratic graphene. Besides, there is no M peak at ~1750 cm⁻¹, which indicates the absence of AB stacked structures.¹



图S5。 (a) N-FG的高分辨率C KLL谱，以及(b)相应的导数曲线。
Figure S5. (a) The high-resolution C KLL spectrum of N-FG, and (b) the corresponding D参数测量微分C KLL俄歇谱中最大值和最小值之间的能量分离，并用于评估sp²和sp³碳的
 衍生曲线。D参数测量微分C KLL俄歇谱中最大值和最小值之间的能量分离，并用于评估sp²和sp³碳的
 相对数量。
 minima in the differentiated C KLL Auger spectrum and is used to evaluate the relative amounts
 1在金刚石(主要是sp³碳)中，D参数值约为13 eV，而由sp²碳组成的石墨的D参数
 of sp² and sp³ carbon.¹ In diamond (mainly sp³-carbon), the D-parameter value is ~13 eV, while
 可达到22 eV。
 graphite, which is comprised of sp²-carbon, has a D-parameter that can reach 22 eV. A larger D-
 D参数越大，
 sp²与sp³的比值越高。
 N-FG的D参数为22.4 eV，与我们之前报告1中的固有FG相似，
 parameter implies a higher sp² to sp³ ratio. The D-parameter for the N-FG is 22.4 eV, which is
 表明N-FG中的主要石墨结构(主要是sp²碳)。
 similar to that of intrinsic FG in our previous report¹ and indicates the dominant graphitic
 structure (mainly sp²-carbon) in N-FG.



图S6。 (a) N-FG的氮吸附和解吸曲线。
Figure S6. (a) Nitrogen adsorption and desorption curves of N-FG. (b) The pore size distribution
 N-FG的表面积为 $303\text{ m}^2\text{ g}^{-1}$, 孔径 $<100\text{ \AA}$ 。
 of N-FG. The surface area of N-FG is $303\text{ m}^2\text{ g}^{-1}$ with pore size $<100\text{ \AA}$.

对于多孔材料，有两种类型的孔，封闭孔和开放孔。
 For the porous materials, there are two types of the pores, closed pores, and open pores.⁴ The
 和开放的含义取决于探针流体(气体或液体)可以扩散到的孔的大小。
 meaning of closed and open depends on the size of the pores into which a probe fluid (gas or
 在任何情况下，当探针流体无法穿透某些空间时，它们被表示为闭合孔。
 liquid) can diffuse. In any case, when the probe fluid cannot penetrate certain spaces, they are
 另一方面，在测量的时间尺度内，探针可以访问的空间将被视为开孔。
 denoted as closed pores. On the other hand, the space that can be accessed by the probe within
 the timescale of the measurement will be regarded as open pores.^{4,5} Since the closed pores are
 应用中无法接近，如钠离子电池或超级电容器电极，因此闭孔不会直接影响电池或电容器的比容量。
 isolated and they cannot be accessed in the electrochemical applications, such as Na-ion batteries
 or supercapacitor electrodes, closed pores do not directly contribute to the specific capacity of
 然而，这些封闭孔确实减少了活性材料的总质量，并有可能增加重量能量密度。
 the batteries or capacitors. However, these closed pores indeed reduce the total mass of the active
 materials and has the potential to increase the gravimetric energy densities.

我们根据前一篇文章中列出的方法计算封闭孔隙度。

We calculate the closed porosity based on the method listed in the previous paper.⁴

$$\rho_s = \frac{m}{V_s + V_c} \quad (3)$$

$$\rho = \frac{m}{V_s} \quad (4)$$

(是材料的骨密度。

ρ_s is the skeletal density of the materials.

是致密(无孔)基质的密度。
 ρ is the density of the dense (pore-free) matrix. $\rho = 2.267 \text{ g cm}^{-3}$
量。
 m is the mass of the materials.

V_s 是稠密矩阵的真实体积。
 V_s is the true volume of the dense matrix.

V_c 是闭合孔隙的体积。
 V_c is the volume of the closed pores.

N-FG的骨密度由以下实验确定。
Skeletal density of N-FG is determined by the experiment below. This analysis assumes that DBM/TCE)混合物可以穿透材料的开孔。
the dibromomethane/tetrachloroethylene (DBM/TCE) mixture can penetrate the open pores of
最初，将N-FG添加到仅填充DBM或仅填充TCE的20 mL小瓶中。
the material. Initially, N-FG was added to a 20 mL vial filled with either only DBM or only
由于N-FG在TCE中下沉，在DBM中漂浮，因此需要中等密度的液体。
TCE. Since the N-FG sank in TCE and floated in DBM, a liquid of intermediate density is
含有大部分悬浮物质的混合物用于N-FG骨密度。
required. The mixture that has most of the material suspended was used for N-FG skeletal
density.

为了求液体混合物的密度，使用以下等式，
To find the density of liquid mixtures, the following equation is used,

$$D_M = \frac{1}{V_M} \cdot ((\rho_{TCE} \cdot V_{TCE}) + (\rho_{DBM} \cdot V_{DBM})) \quad (5)$$

/01和23。是TCE和DBM的密度。
 ρ_{TCE} and ρ_{DBM} are the densities of TCE and DBM. $\rho_{TCE} = 1.625 \text{ g cm}^{-3}$ and $\rho_{DBM} = 2.477 \text{ g cm}^{-3}$. The final ratio $V_{TCE}:V_{DBM} = 10:1$

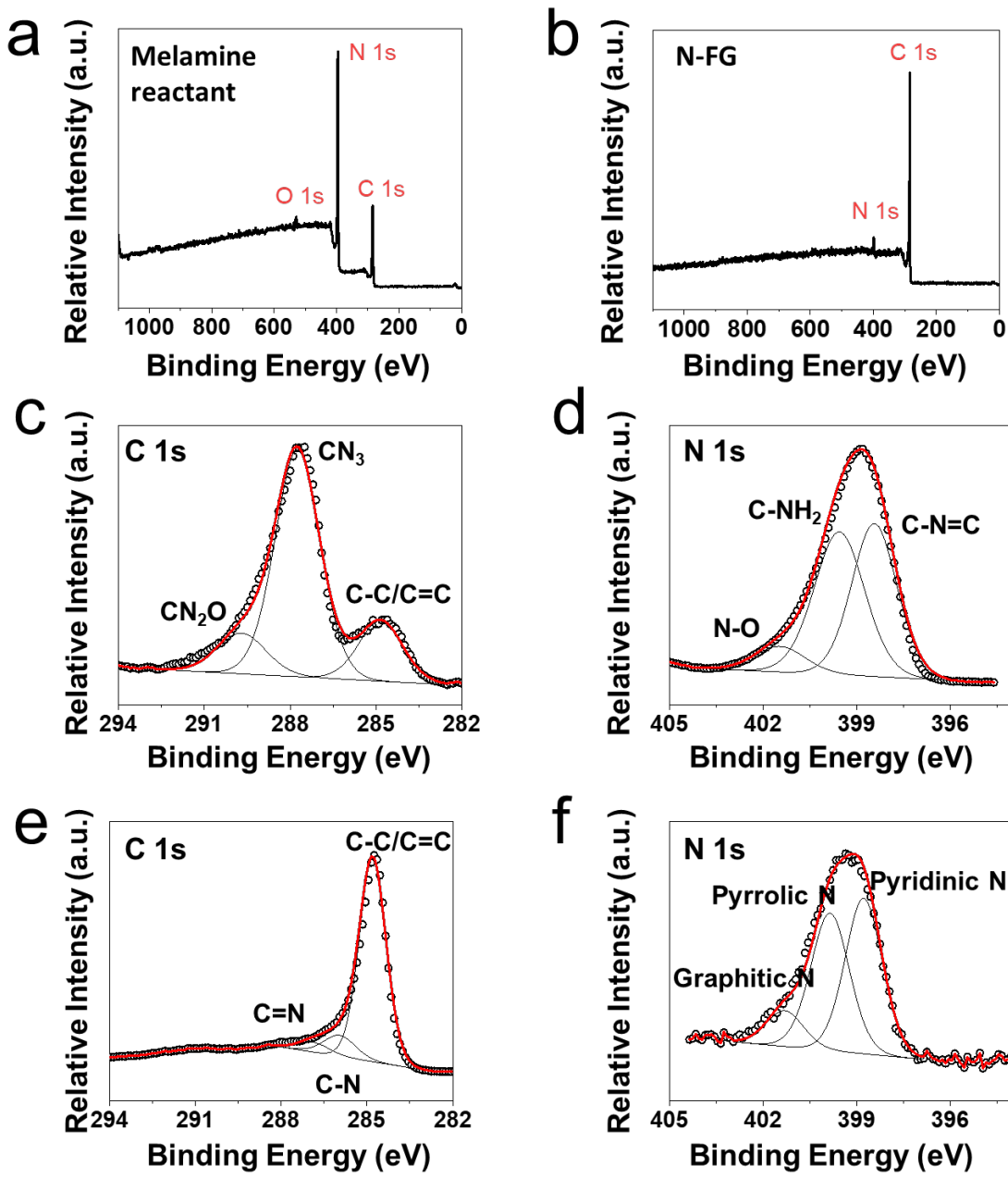
因此，N-FG的骨密度为 1.702 g cm^{-3} 。
Therefore, the skeletal density of N-FG is 1.702 g cm^{-3} .

根据图S6中的BET数据，开孔体积为#=0.692-，&。
From the BET data in Figure S6, the volume of the open pores is $V_o = 0.692 \text{ cm}^3 \text{ g}^{-1}$. The
孔隙度和开放孔隙度可通过以下等式计算。
closed porosity and open porosity can be calculated by the following equations.⁴

封闭孔隙度 $\epsilon_c = \frac{V_c}{V_c + V_s + V_o}$ ！
The closed porosity $\epsilon_c = \frac{V_c}{V_c + V_s + V_o}$ (6)

开口孔隙度 $\epsilon_o = \frac{V_o}{V_c + V_s + V_o}$ ！
The open porosity $\epsilon_o = \frac{V_o}{V_c + V_s + V_o}$ (7)

因此，闭合孔隙度为0.11，开放孔隙度为0.54。
Therefore, the closed porosity is 0.11 and the open porosity is 0.54.



图S7。 (a)三聚氰胺反应物和(b)合成的N-FG样品的测量光谱。

Figure S7. The survey spectra of (a) melamine reactant and (b) as-synthesized N-FG sample.

(c, d)三聚氰胺反应物和(e, f)N-FG样品的C 1s和N 1s的高分辨率XPS光谱。

High resolution XPS spectra of C 1s and N 1s for (c, d) melamine reactant and (e, f) N-FG

N-FG含有氮和碳。

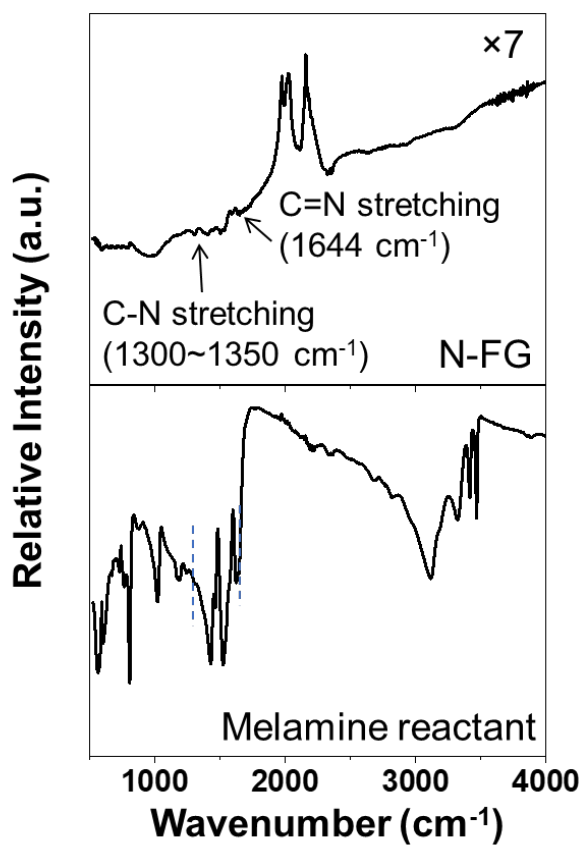
3个不同批次的氮掺杂含量分别约为5.4%、5.0%和5.5%。

sample. N-FG has nitrogen and carbon. The N doping contents from 3 different batches are

~5.4%, ~5.0% and ~5.5%, respectively. The deconvoluted result shows the formation of C-N)的形成，它们在反应物中不存在，并指示转化

(~285.9 eV) and C=N (~286.9 eV), which are absent in the reactant and indicate the conversion

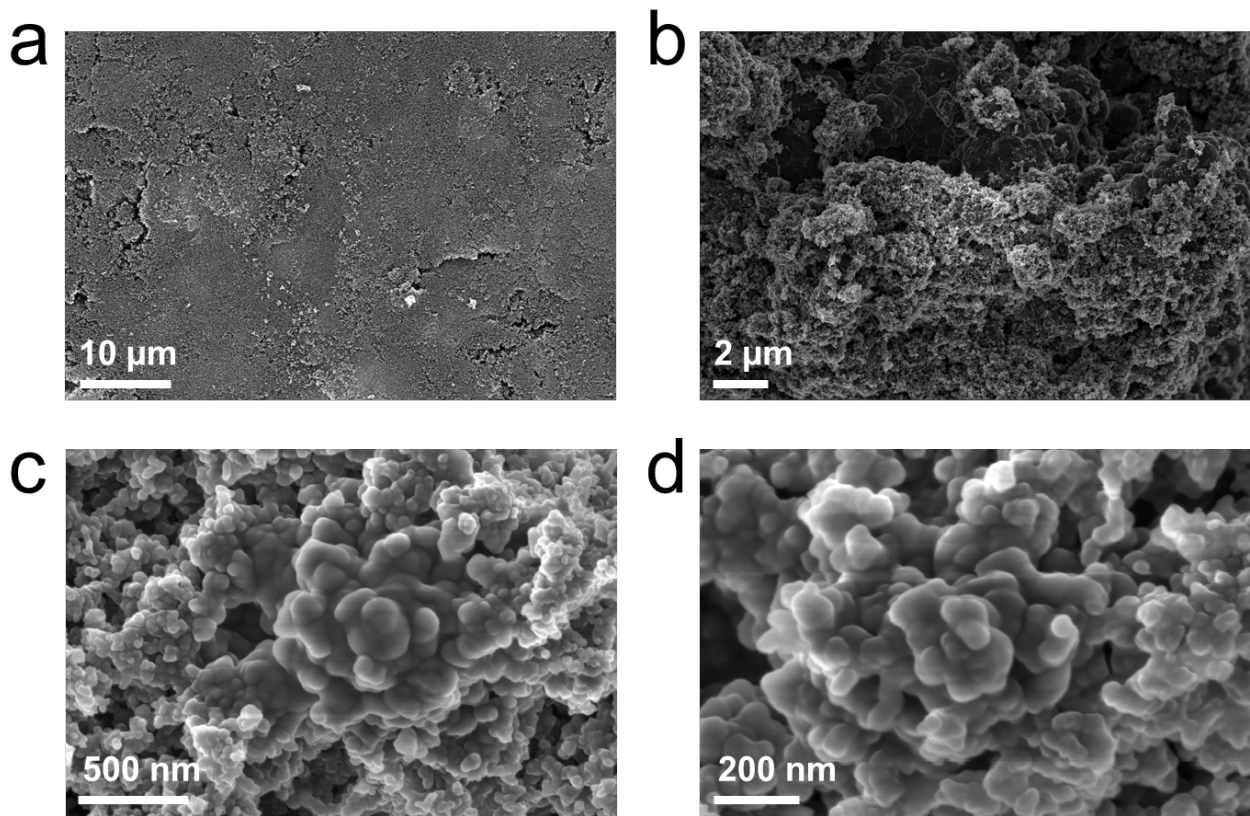
三聚氰胺反应物。 氮以吡啶氮(约398.7 eV)、吡咯氮(约399.8 eV)和石墨氮(约401.2 eV)的形式存在。
of the melamine reactant. The N exists in the form of pyridinic N (~398.7 eV), pyrrolic N (~399.8 eV) and graphitic N (~401.2 eV).



图S8。N-FG和三聚氰胺反应物的FTIR光谱。

Figure S8. FTIR spectra of N-FG and melamine reactant. The spectrum of N-FG was magnified

N-FG样品中不存在三聚氰胺峰以及C-N和C=N拉伸峰的信号证实了FJH过程中~7× for a better demonstration. The absence of melamine peaks and the signal of C-N and C=N的氮掺杂。stretching peaks in N-FG sample confirm the nitrogen doping during FJH process.

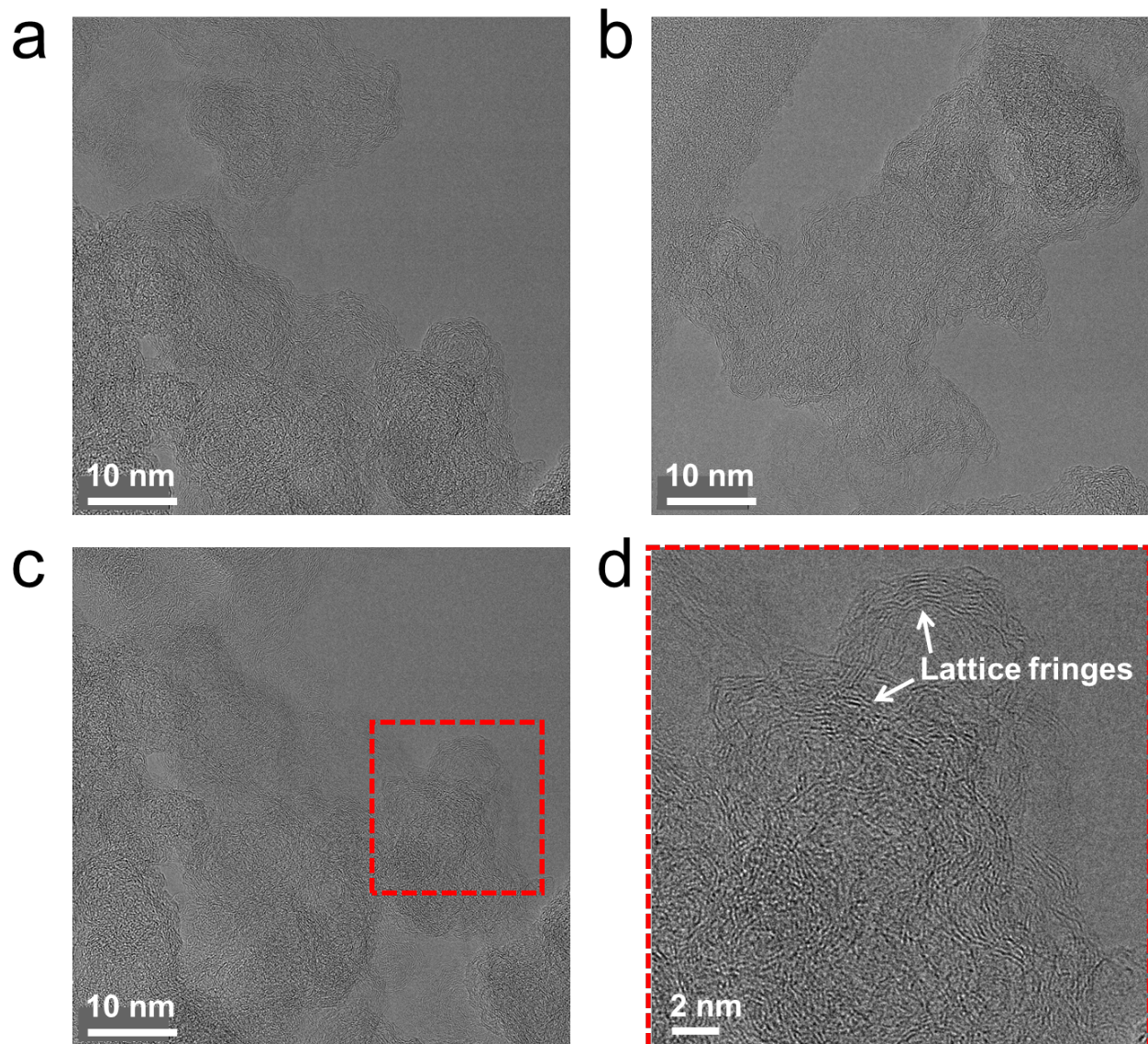


图S9。N-FG纳米晶体的SEM图像。

从SEM图像中测量了100个石墨烯片的尺寸分布。

Figure S9. The SEM images of N-FG nanocrystals. The size distribution of 100 graphene sheets

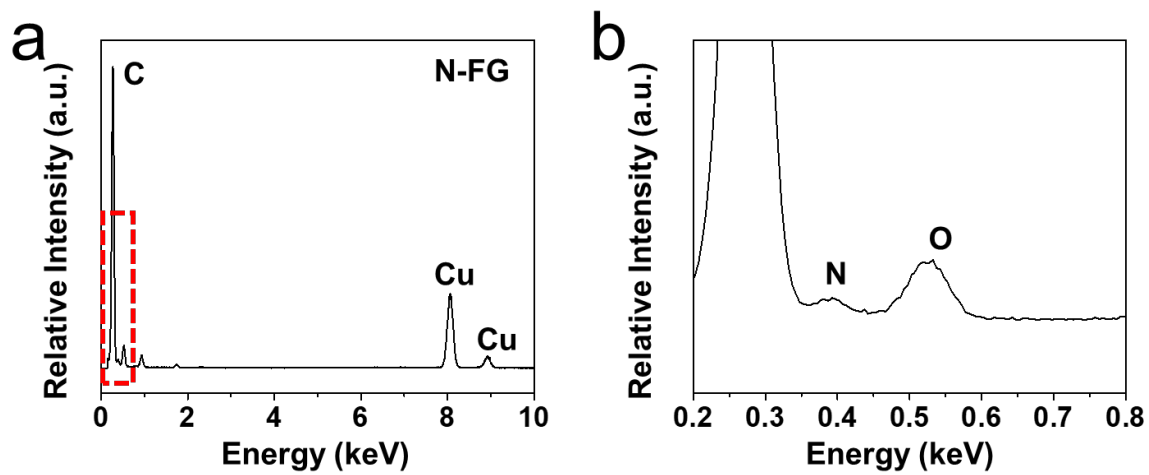
is measured from SEM images.



图S10。N-FG的HR-TEM图像。

Figure S10. The HR-TEM images of N-FG. The graphene lattice fringes, and the jagged structure of graphene nanocrystals, can be distinguished from the HR-TEM images.

石墨烯晶格条纹和石墨烯纳米晶体的锯齿结构可以从

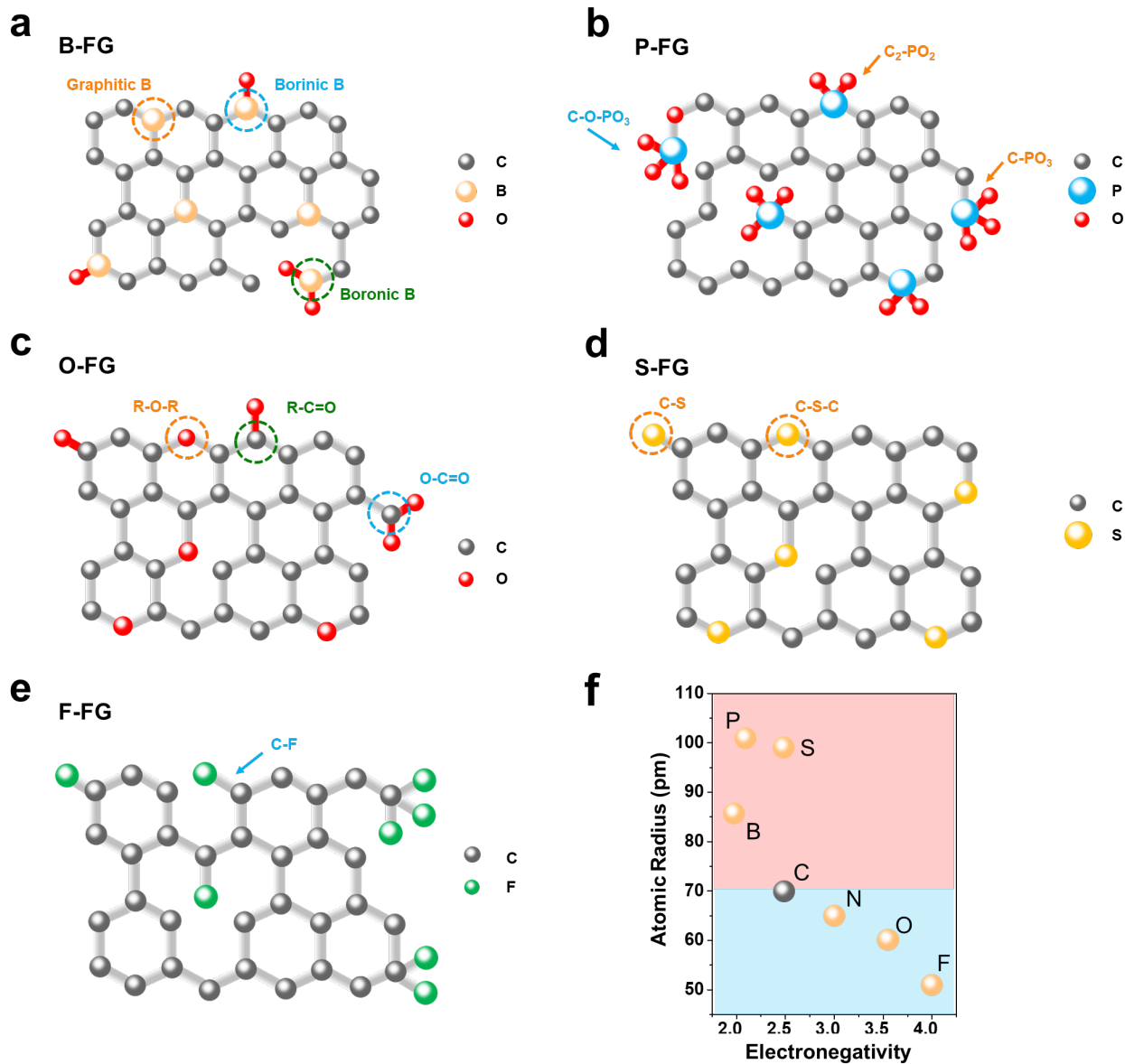


图S11。通过TEM-EDS对N-FG进行元素分析。

Figure S11. Elemental analysis of N-FG by TEM-EDS. Figure S11b is the magnified plot of the specific boxed region shown in Figure S11a.

杂原子掺杂闪光石墨烯的表征

Characterization of heteroatom-doped flash graphene



图S12。杂原子掺杂闪光石墨烯的示意图。

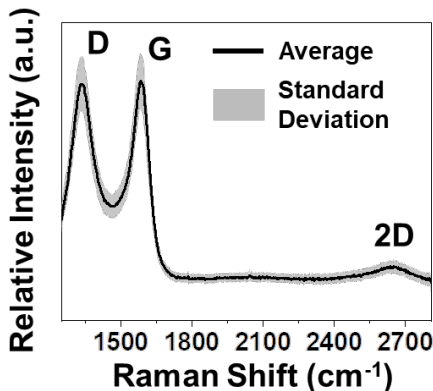
Figure S12. The schematic of heteroatom-doped flash graphene. (a) B-FG. (b) P-FG. (c) O-FG.

在石墨结构中证明了每个杂原子与碳原子的重要键合状态。

(d) S-FG. (e) F-FG. The important bonding states of each heteroatom with carbon atom are

(f) 各种掺杂剂相对于碳的电负性和原子半径。

demonstrated in the graphitic structures. (f) The electronegativities and atomic radii of various dopants relative to carbon.



图S13。非晶碳的统计拉曼光谱。

Figure S13. The statistic Raman spectra of the amorphous carbon. The black line and the gray shadow represent the average value and the standard deviation of 100 sampling points, respectively.

各种杂原子掺杂FG的石墨烯含量产率的计算基于2D/G强度比。

The calculation of graphene content yield for various heteroatom-doped FG is based on the 2D/G intensity ratios. Since the average value of I_{2D}/I_G for amorphous carbon as shown in Figure 0.10的阈值来确定材料是否为石墨烯。

S13 is 0.06 and the largest value can reach 0.07, a threshold value of 0.10 is used to determine if

使用超过100个采样点的拉曼映射来确定石墨烯含量产率。

the material is graphene or not. Raman mapping over 100 sampling points is used to determine

the graphene content yield.

具体来说，对于单个采样点，

Specifically, for a single sampling point,

1) 如果 $I_{2D}/I_G > 0.10$ ，则样品为石墨烯。

1) The sample is graphene if $I_{2D}/I_G > 0.10$.

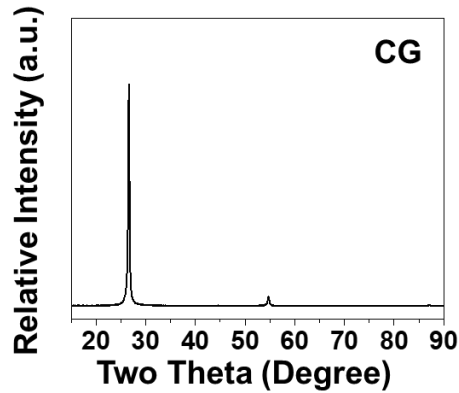
2) 如果 $I_{2D}/I_G < 0.10$ ，则样品不是石墨烯。

2) The sample is not graphene if $I_{2D}/I_G < 0.10$.

各种杂原子掺杂FG的质量产率的计算基于起始材料的重量和我们可以从闪速反应中收集的产物的重量。

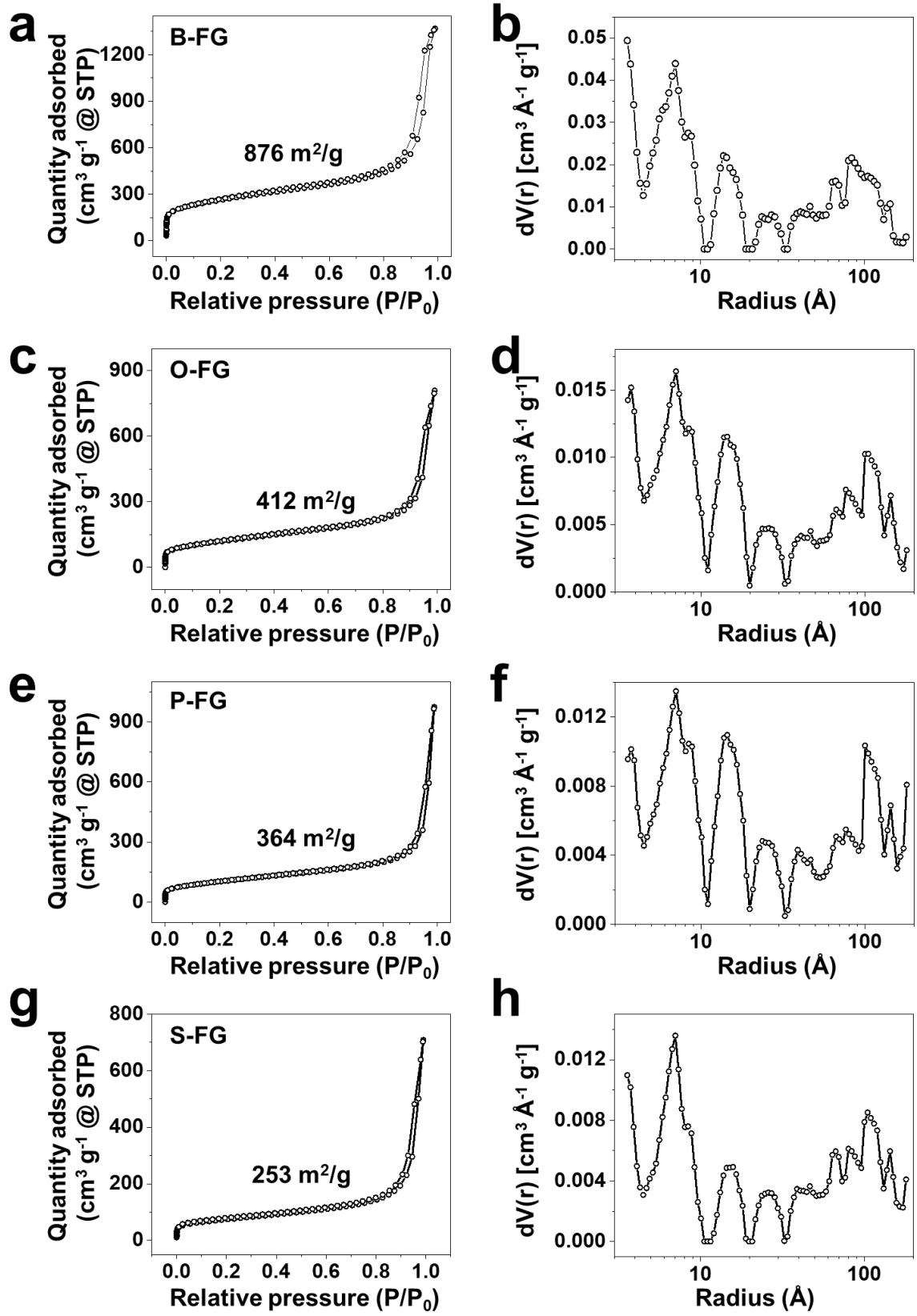
The calculation of mass yield for various heteroatom-doped FG is based on the weight of starting materials and the weight of products we can collect from the flash reaction. Specifically, it can be calculated by eq 8 below.

$$\text{mass yield} = \frac{\text{Weight of product}}{\text{Weight of starting material}} \quad (8)$$



图S14。商业石墨烯纳米板(CG)的XRD结果。

Figure S14. The XRD result of commercial graphene nanoplates (CG).



图S15。 (a , c , e , g) 氮吸附和脱附曲线和(b , d , f , h)各种杂原子掺杂FG的孔径分布。

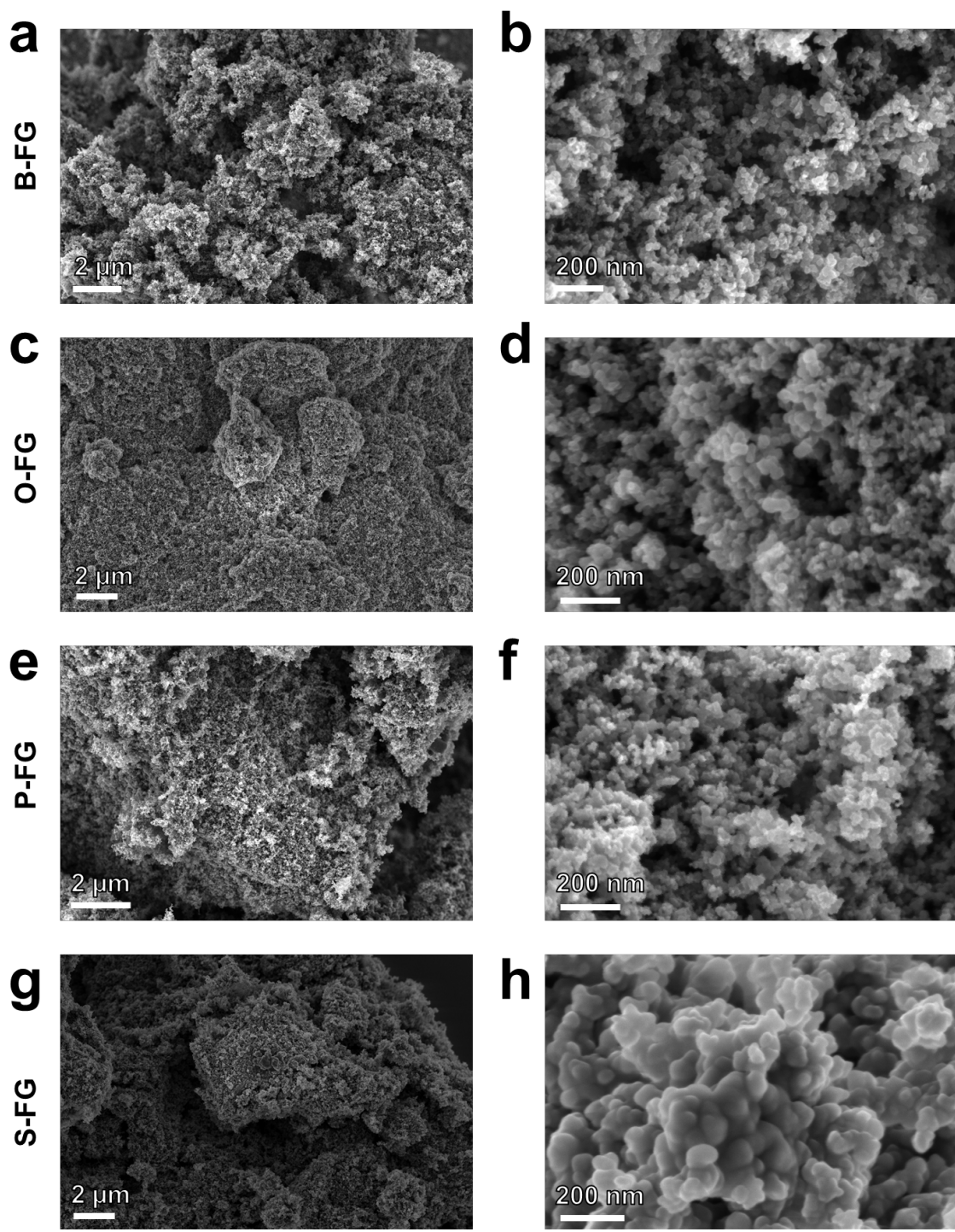
Figure S15. (a, c, e, g) Nitrogen adsorption and desorption curves and (b, d, f, h) the pore size

distribution of various heteroatom-doped FG. (a, b) B-FG. (c, d) O-FG. (e, f) P-FG. (g, h) S-FG.

孔径分布结果表明，不同类型的杂原子掺杂FG具有丰富的微孔和中孔。

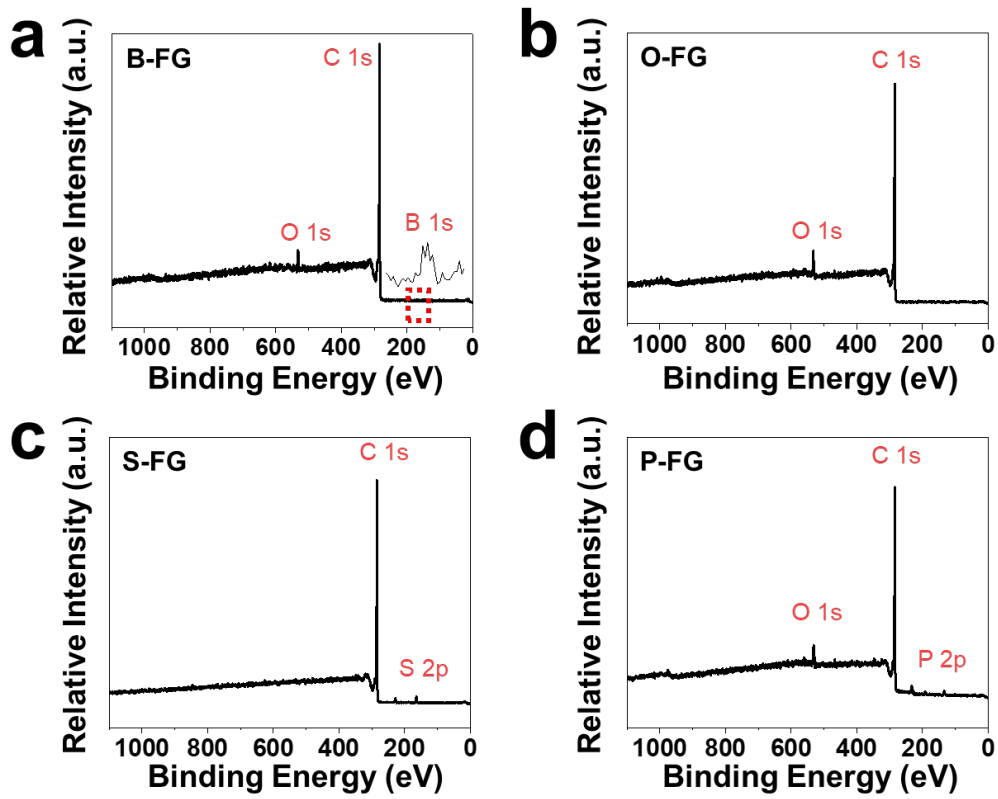
The pore size distribution results indicate that there are abundant micropores and mesopores for

different types of heteroatom-doped FG.



图S16。不同杂原子掺杂FG的SEM图像。

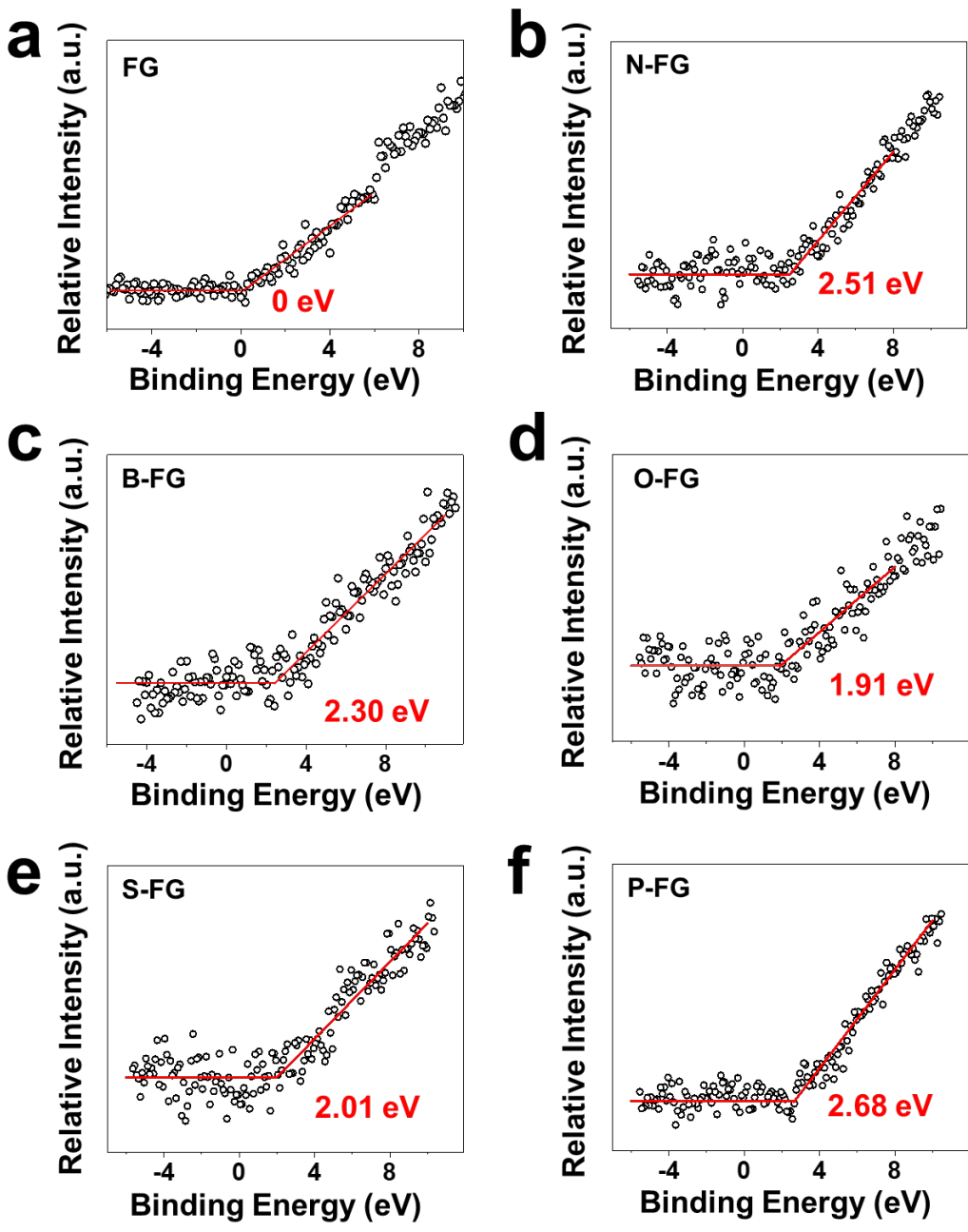
Figure S16. The SEM images of different heteroatom-doped FG. (a, b) B-FG. (c, d) O-FG. (e, f) P-FG. (g, h) S-FG.



图S17。 杂原子掺杂FG的XPS测量光谱。

Figure S17. The XPS survey spectra of heteroatom-doped FG. (a) B-FG. The inset shows the enlarged area of B 1s, which is denoted by the red dashed box. (b) O-FG. (c) S-FG. (d) P-FG.

插图显示了B 1s的放大

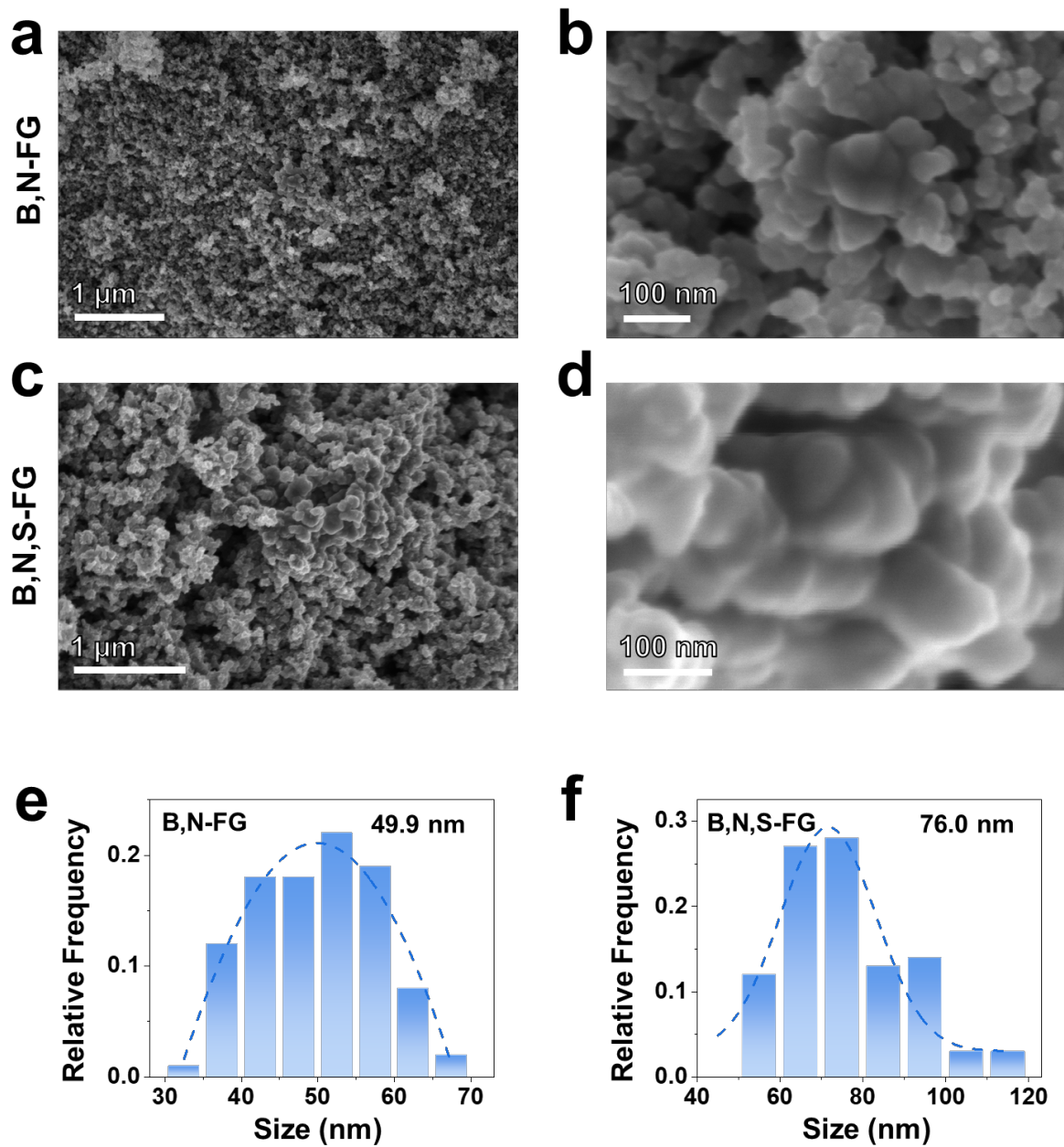


图S18。各种杂原子掺杂FG的价带XPS结果。

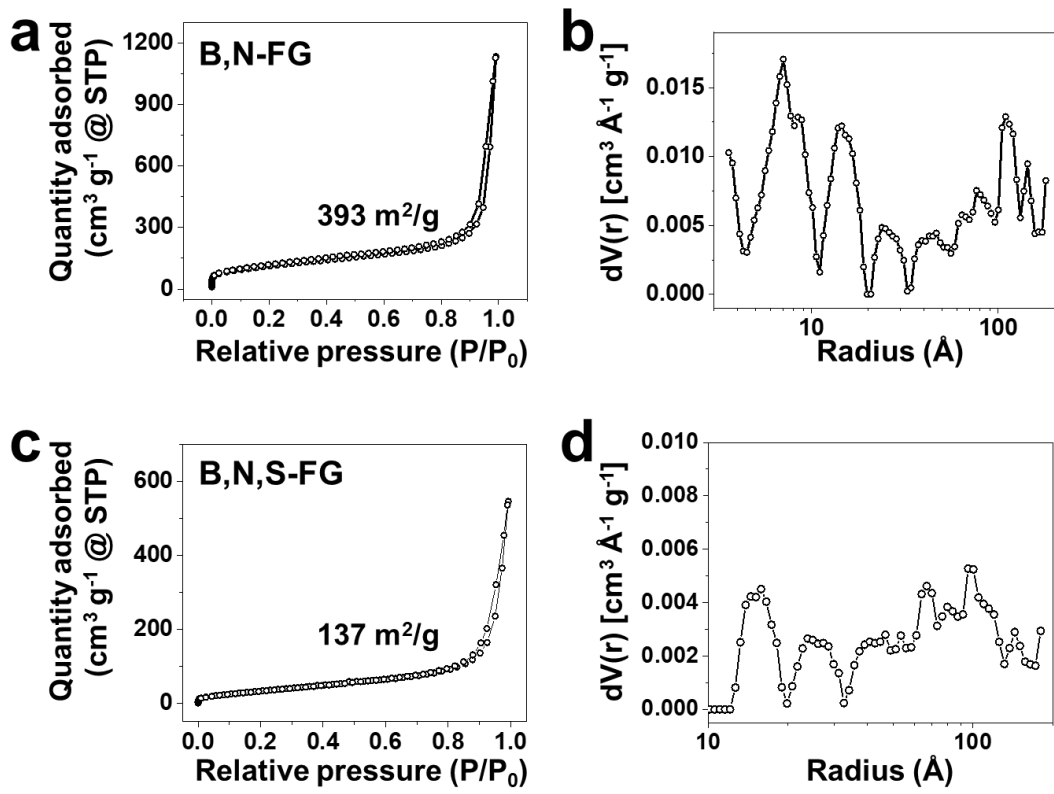
Figure S18. The valence band XPS results of various heteroatom-doped FG. (a) FG. (b) N-FG.

(c) B-FG. (d) O-FG. (e) S-FG. (f) P-FG.

异质原子共掺杂闪光石墨烯的表征
Characterization of heteroatoms co-doped flash graphene



图S19。杂原子共掺杂FG的SEM图像。
Figure S19. The SEM images of heteroatom co-doped FG. (a, b) B,N-FG. (c, d) B,N,S-FG. (e) B , N , S-FG的尺寸分布。 (f) B , N , S-FG的尺寸分布。
The size distribution of B,N-FG. (f) The size distribution of B,N,S-FG.



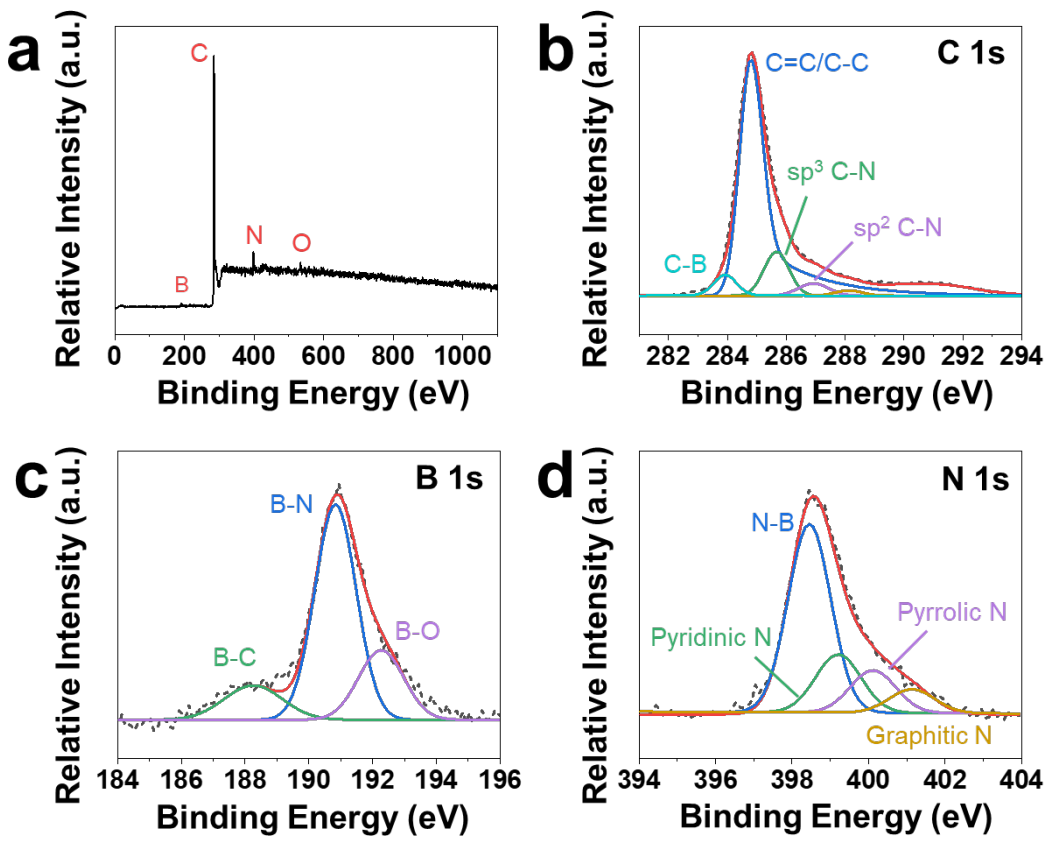
图S20。(a, c)氮吸附和解吸曲线以及(b, d)各种杂原子掺杂FG的孔径分布。

Figure S20. (a, c) Nitrogen adsorption and desorption curves and (b, d) the pore size distribution

of various heteroatom-doped FG. (a, b) B,N-FG. (c, d) B,N,S-FG. The pore size distribution

杂原子共掺杂FG具有丰富的微孔和中孔。

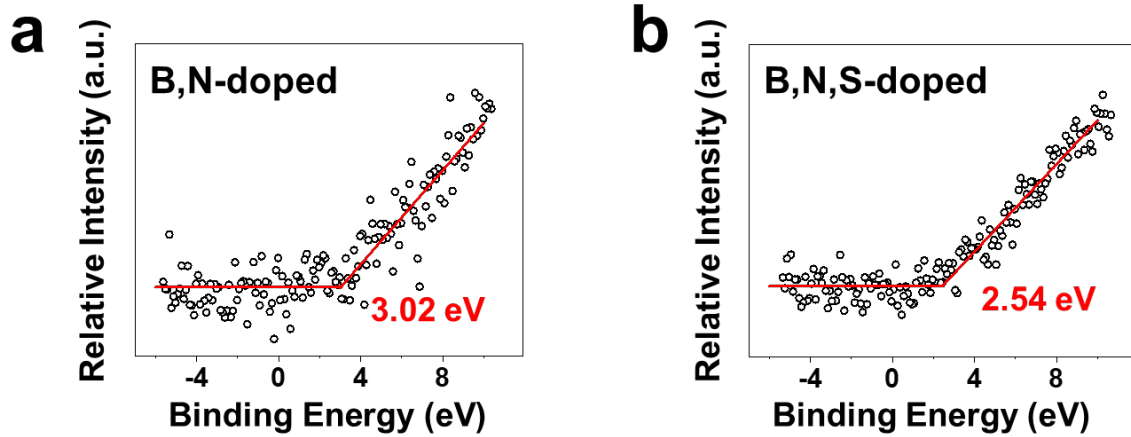
results indicate that there are abundant micropores and mesopores for different types of heteroatom co-doped FG.



图S21。B, N-FG的元素分析。

Figure S21. The elemental analysis of B,N-FG. (a) Survey spectrum. High-resolution spectra of (b) C 1s, (c) B 1s and (d) N 1s光谱的高分辨率光谱。

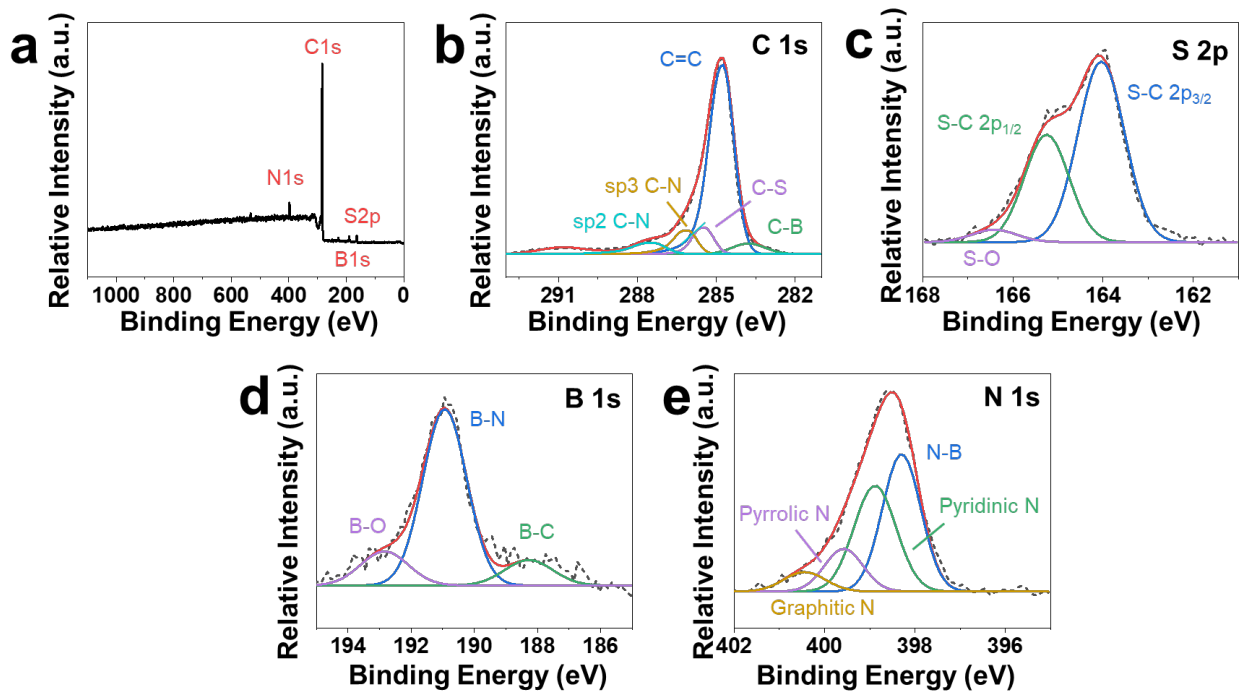
(b) C 1s, (c) B 1s and (d) N 1s spectra.



图S22。 各种杂原子共掺杂FG的价带XPS结果。

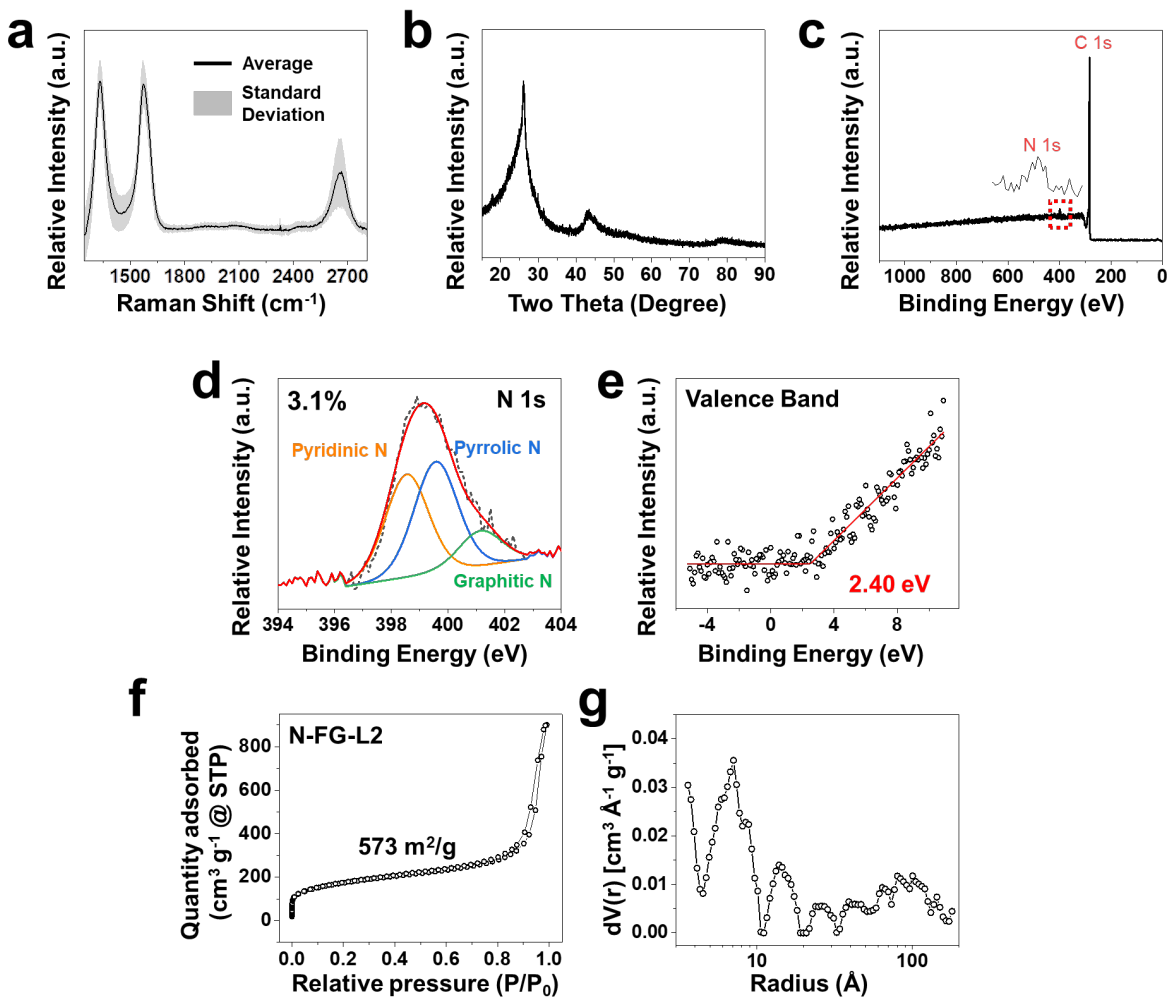
Figure S22. The valence band XPS results of various heteroatom co-doped FG. (a) B,N-FG. (b)

B,N,S-FG.

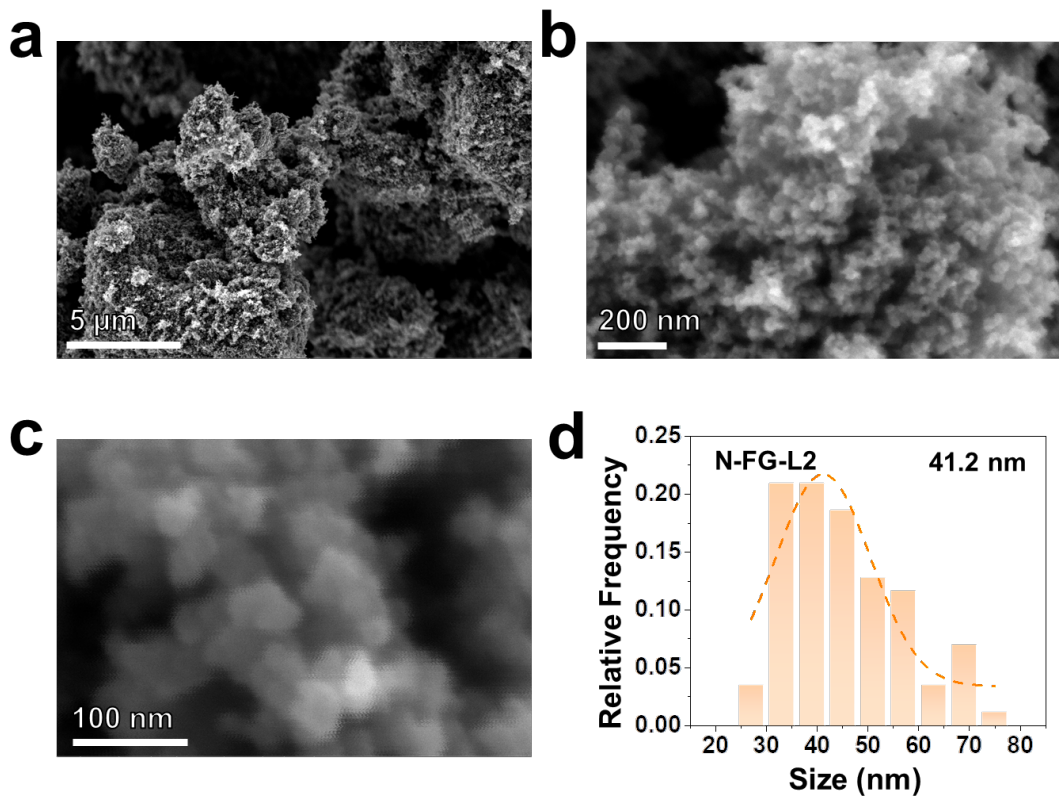


图S23。B , N , S-FG的元素分析。
Figure S23. The elemental analysis of B,N,S-FG. (a) Survey spectrum. High-resolution spectra
 of (b) C 1s, (c) S 2p (d) B 1s and (e) N 1s spectra.

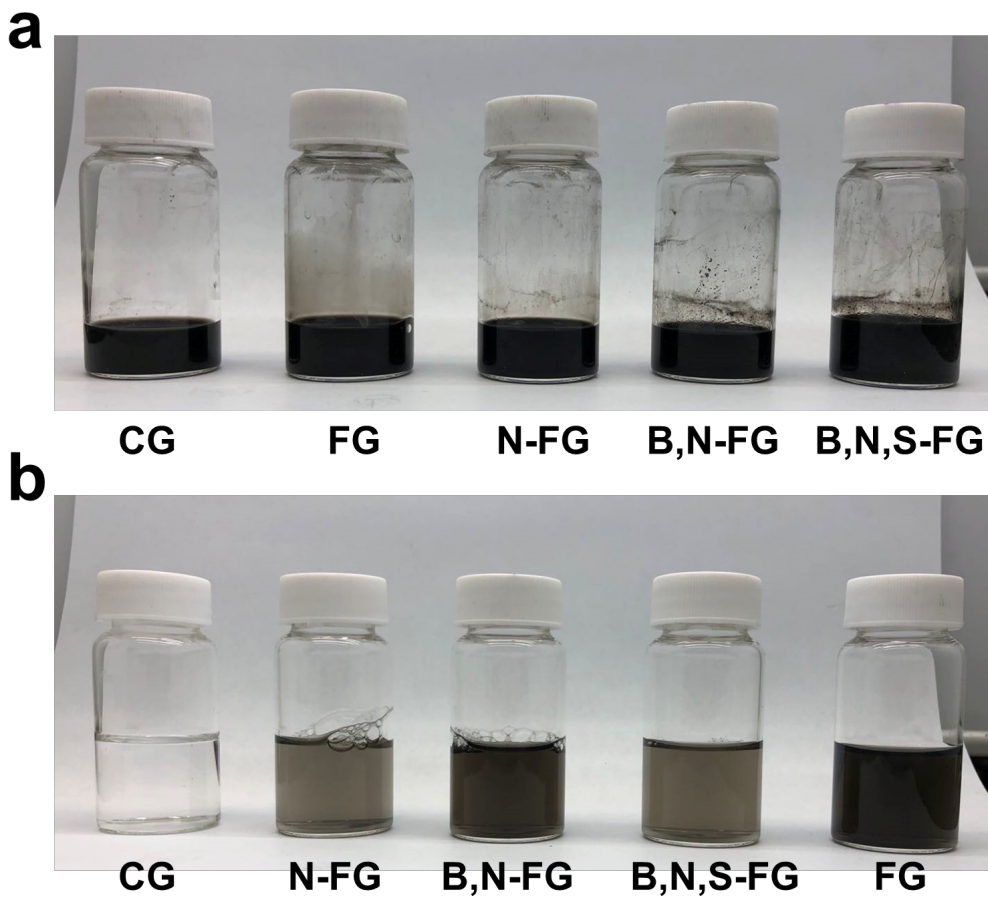
杂原子掺杂闪光石墨烯的放大及应用
Scaling up and applications of heteroatom-doped flash graphene



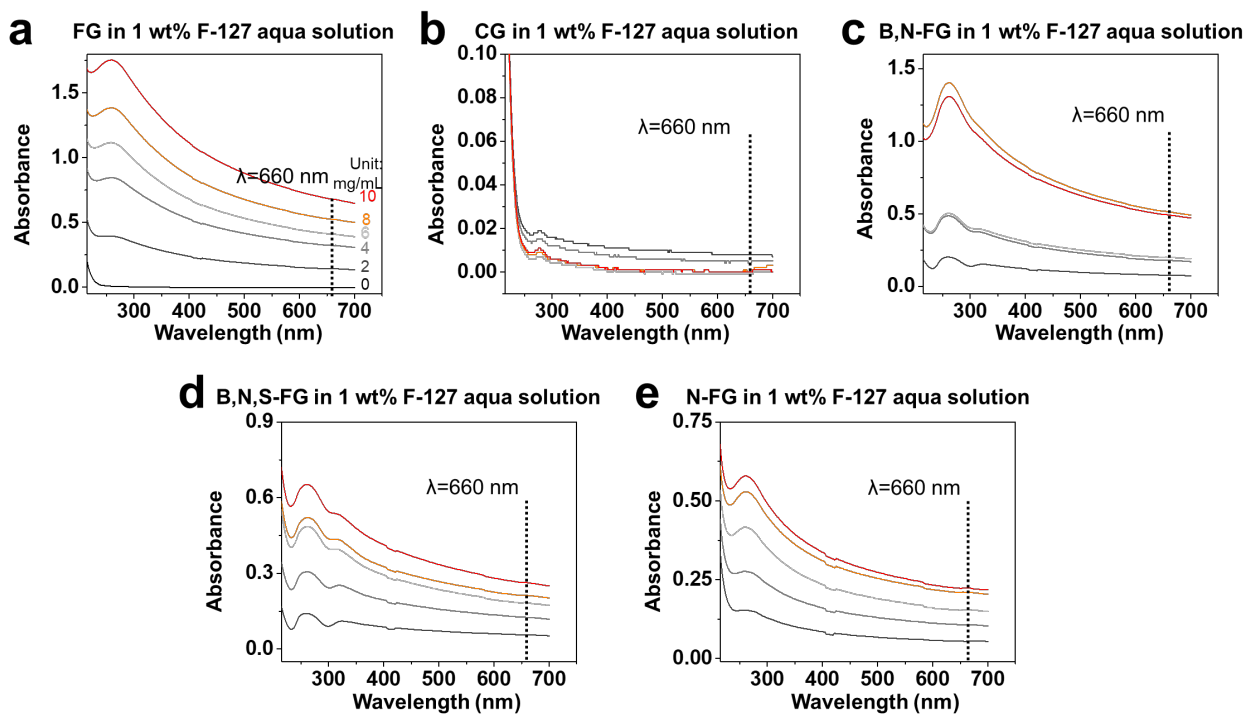
图S24。N-FG的放大。
Figure S24. Scaling up of N-FG. The characterization of N-FG prepared in large scale (1 g batch, N-FG-L2). (a) Statistic Raman spectra of N-FG-L2. The black line and the gray shadow represent the average value and the standard deviation of 100 sampling points, respectively. (b) XRD result of N-FG-L2. (c) Survey spectrum of N-FG-L2. (d) High-resolution spectra of N 1s价带。(e) valence band of N-FG-L2. (f) Nitrogen adsorption and desorption curves of N-FG-L2. (g) N-FG-L2的孔径分布。
N-FG的表面积为 $573 \text{ m}^2 \text{ g}^{-1}$, 孔径 $<100 \text{ \AA}$ 。



图S25。N-FG-L2的形态。(a-c)N-FG-L2的SEM图像和(d)相应的尺寸分布。
Figure S25. The morphology of N-FG-L2. (a-c) SEM images of N-FG-L2 and (d) corresponding size distribution.



图S26。 (a) 各种掺杂杂原子的FG分散在浓度为 10 g L^{-1} 的水Pluronic(F-127)(1%)溶液中，以及(b)稀释500倍后的分散体的光学图像。
Figure S26. The optical images of (a) various heteroatom-doped FG dispersed in water–Pluronic (F-127) (1%) solution at concentration of 10 g L^{-1} and (b) the dispersions after being diluted 500 times.

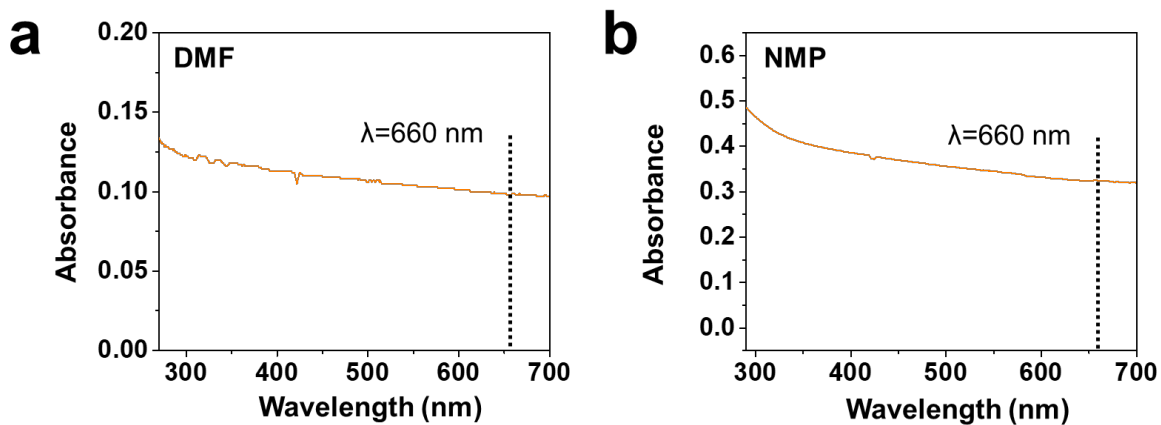


图S27。 在浓度为2-10g/L的水溶液中，各种杂原子掺杂的FG的吸收光谱。(a) 前景。

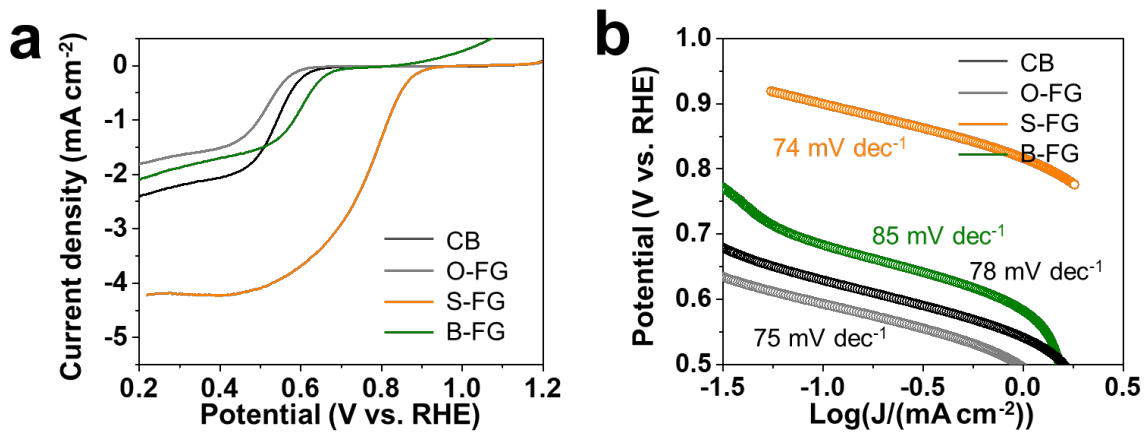
Figure S27. The absorbance spectra of various heteroatom-doped FG dispersed in water-

Pluronic (F-127) (1%) solution at concentration of 2-10 g L⁻¹. (a) FG. (b) CG. (c) B,N-FG.(d)

在进行紫外-可见光谱分析之前，将所有溶液稀释500倍。
B,N,S-FG. (e) N-FG. All the solutions are diluted 500 times before the UV-Vis analyses.



图S28。 N-FG分散在浓度为10 g L⁻¹的普通有机溶液中的吸收光谱。**(a)** N,N-二甲基甲酰胺(
Figure S28. The absorbance spectra of N-FG dispersed in common organic solutions at a
concentration of 10 g L⁻¹. (a) N,N-Dimethylformamide (DMF). (b) *N*-Methyl-2-pyrrolidone
(NMP)。与DMF和NMP溶液中的CG相比，N-FG的色散效率分别高出约40.4倍和约8.2倍。
(NMP). Compared to the CG in DMF and NMP solutions, the dispersion efficiencies of N-FG
are ~40.4 and ~8.2 times higher.

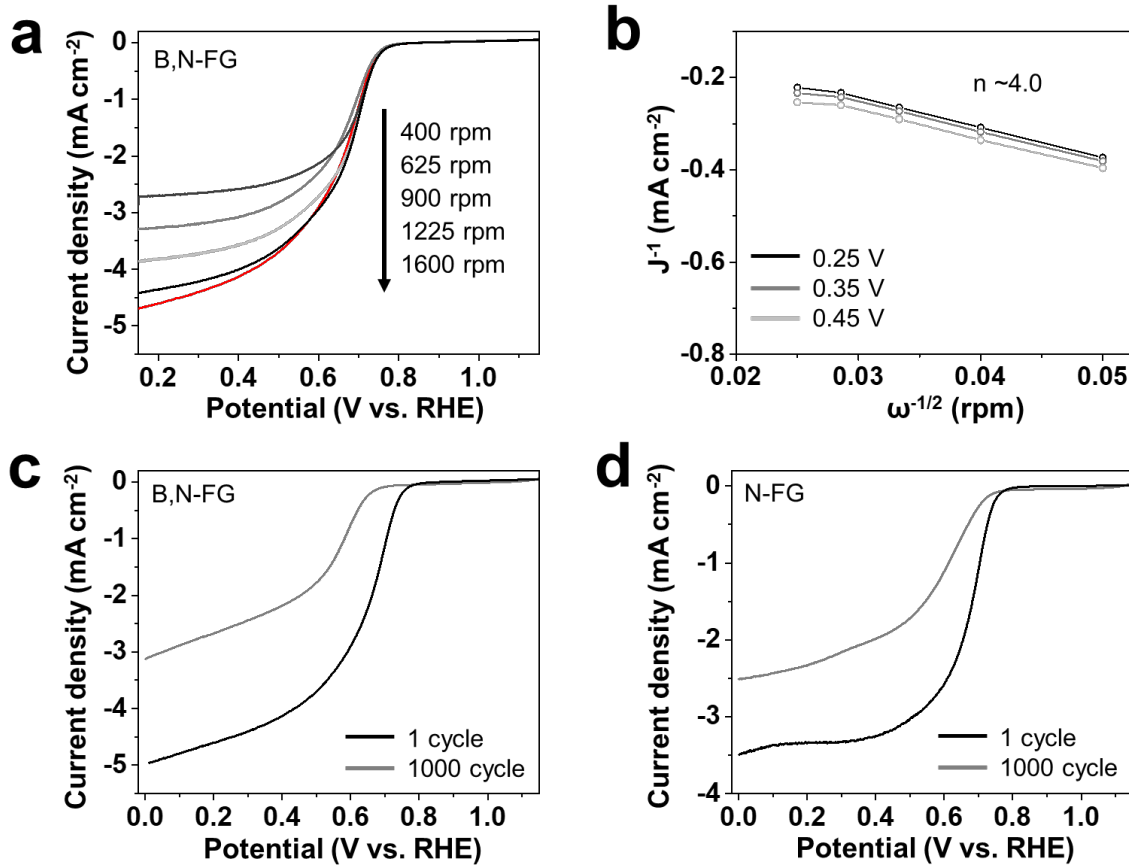


图S29。(a) 不同掺杂FG和本征FG在1600 rpm下0.1 M KOH溶液中的氧还原反应(ORR)性能。

Figure S29. (a) Oxygen reduction reaction (ORR) performance of different doped FG and

(b) 相应的塔菲尔图。

intrinsic FG in 0.1 M KOH solution at 1600 rpm. (b) Corresponding Tafel plots.



图S30。 (a) B、N-FG和(B)对应的K-L图在不同转速下的ORR极化曲线。
Figure S30. (a) The ORR polarization curves at different rotating rates of B,N-FG and (b) corresponding K-L plots. The electron transfer number (n) is close to 4.0 for B,N-FG, which indicates H_2O is the major product here. Durability of (c) B,N-FG and (d) N-FG showing the polarization curve for the 1st cycle and the 1000th cycle.

Koutecky-Levich方程
Koutecky–Levich equation

氧还原电流遵循Koutecky-Levich方程(K-L方程),²⁷

The oxygen reduction current follows Koutecky–Levich equation (K-L equation),²⁷

$$J^{-1} = J_K^{-1} + J_L^{-1} \quad (9)$$

J 是电势相关的动力学电流密度, J_L 是Levich扩散极限电流密度。
 J is the total current density (mA cm^{-2}). J_K is the potential dependent kinetic current density and J_L is the Levich diffusion-limiting current density.

$$J_L = B \omega^{1/2} \quad (10)$$

电子转移数(n)可以从400到1600 rpm的不同转速()下的ORR极化曲线计算得出，
The electron transfer number (n) can be calculated from the ORR polarization curves at

different rotating rates (ω) from 400 to 1600 rpm,

$$B = 0.2nFC_0(D_O)^{2/3}\nu^{-1/6} \quad (11)$$

F是法拉第常数(~ 96485 C/mol)

F is the Faraday constant (~96485 C/mol)

C_o 是O₂的体积浓度(~ 1.2×10^{-6} mol/cm³)。

C_o is the bulk concentration of O₂ (~ 1.2×10^{-6} mol/cm³).

D_O 是O₂在0.1 M KOH溶液中的扩散系数(~ 1.9×10^{-5} cm²/s)。

D_O is the diffusion coefficient of O₂ in 0.1 M KOH solution (~ 1.9×10^{-5} cm²/s).

ν 是电解质的运动粘度(0.01 cm²/s)。

ν is the kinematic viscosity of the electrolyte (0.01 cm²/s).

在一定电位下，反向总电流密度(j^{-1})与圆盘电极转速的倒数根(-1/2)的关系如图5g和图S30所示。

The inverse total current density (j^{-1}) vs the reciprocal root of rotating speed of the disk

electrode ($\omega^{-1/2}$) under a certain potential is shown in Figure 5g and Figure S30. The slope (1/B) 斜率(1/B)通过
数据点的线性拟合计算得出。
is calculated from the linear fitting of the data points.

样品消解和ICP-MS测量

Sample digestion and ICP-MS measurement

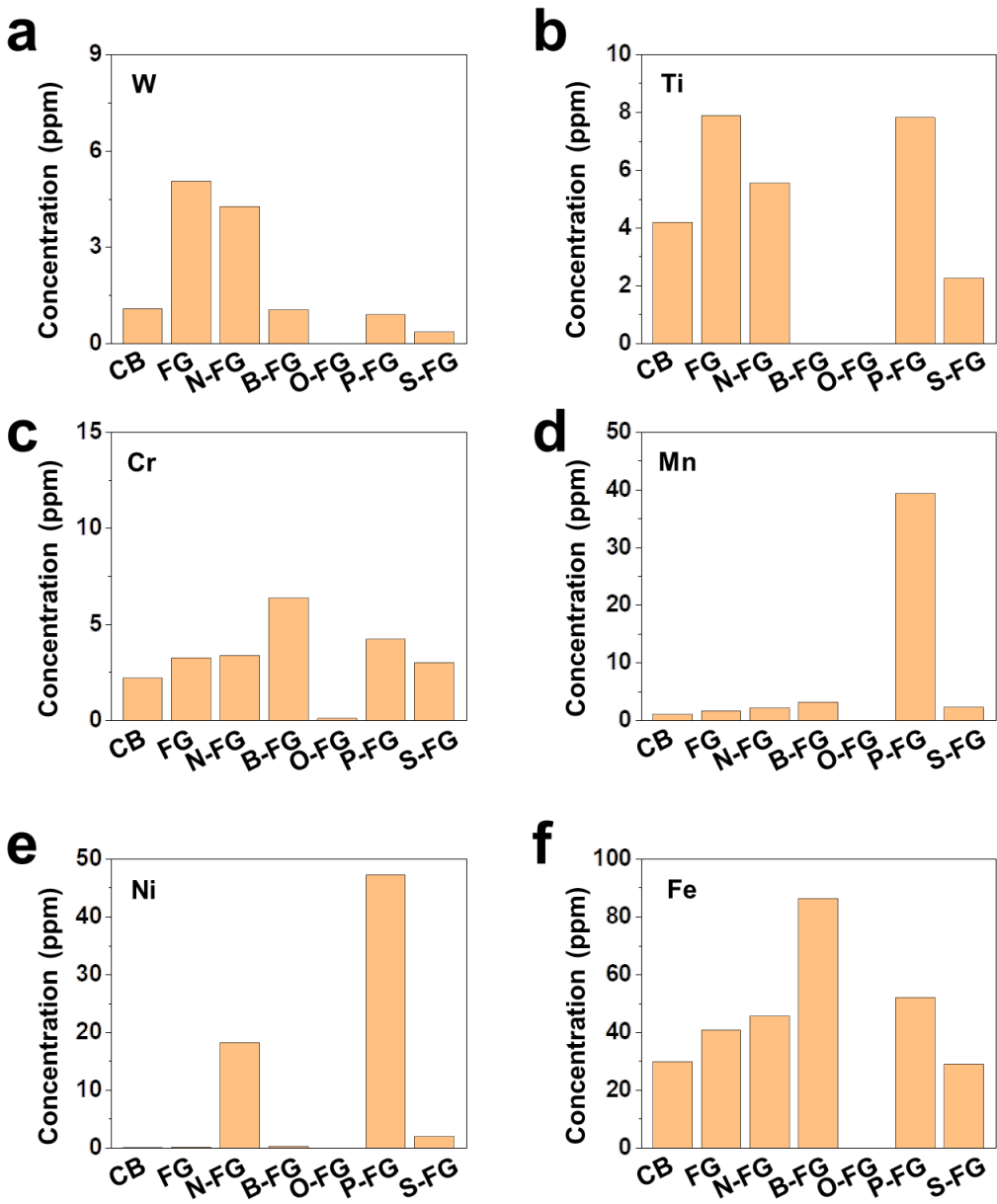
本节中，**HNO₃(67-70 wt%，TraceMetal™级，费希尔化学)**、**HCl(37 wt%，99.99%微量金属基，微孔HNO₃(67–70 wt%，TraceMetal™ Grade, Fisher Chemical)**，**HCl(37 wt%，99.99% trace西格玛)和水(微孔西格玛，ACS超痕量分析试剂)**用于样品消解。
metals basis, Millipore-Sigma), and water (Millipore-Sigma, ACS reagent for ultratrace analysis)

所有掺杂原子的FG样品均采用稀释王水法进行消解。
are used for sample digestion in this section. All the heteroatom-doped FG samples are digested

28将样品浸泡在HNO₃/HCl(各1 M)溶液中
using a dilute *aqua regia* method.²⁸ The samples are soaked in HNO₃/HCl (1 M each) solution at 85 °C持续6小时过滤酸性溶液以去除任何未溶解的颗粒。
85 °C for 6 h. The acidic solution was filtered to remove any undissolved particles. The solution内使用2 wt%HNO₃将溶液稀释至适当的浓度范围。

was then diluted to the appropriate concentration range using 2 wt% HNO₃ within the calibration

ICP-MS使用Perkin Elmer Nexion 300 ICP-MS系统进行。然后在校准曲线
curve. ICP-MS was conducted using a Perkin Elmer Nexion 300 ICP-MS system. The CB, FG,
杂杂原子的FG使用相同的协议进行消化。
and various heteroatom-doped FG are digested using the same protocol.



图S31。

通过电感耦合等离子体质谱(ICP-MS)测定杂原子掺杂FG中各种痕量金属的浓度。

Figure S31. The concentration of various trace metals in heteroatom-doped FG as determined by

inductively coupled plasma mass spectrometry (ICP-MS). For the above six different transition

Mn、Ni和Fe，其浓度比以前文献中报道的浓度低1~3个数量级。

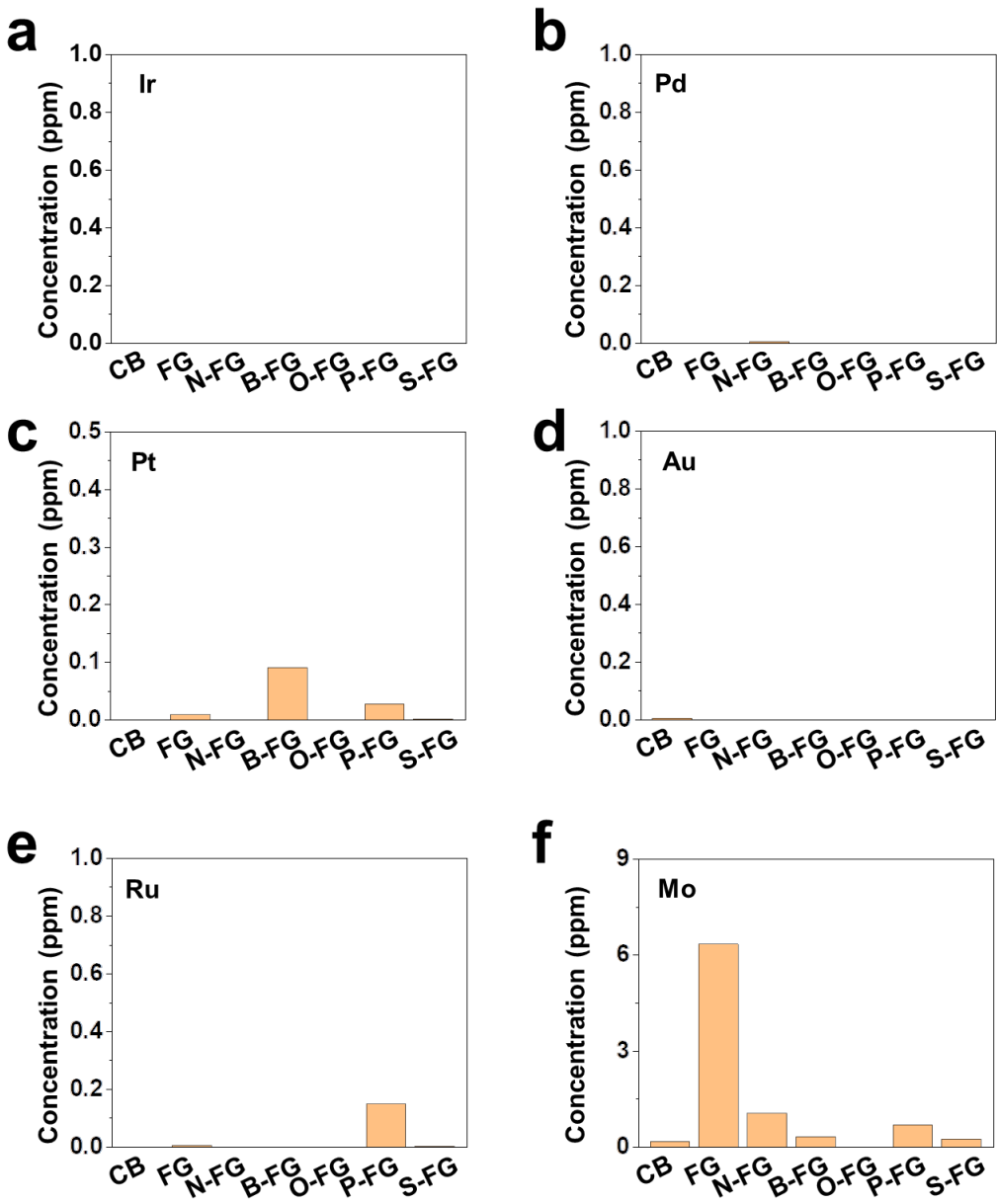
metals, W, Ti, Cr, Mn, Ni and Fe, the concentrations are 1~3 orders of magnitude lower than the

29-31此外，这些过渡金属的浓度与杂原子掺杂FG的催化性能之间没有明显的关系。

between the concentrations of these transition metals and the catalytic performance of the

这些发现表明，金属含量对ORR的影响最小。

heteroatom-doped FG. These findings suggest minimal effect of metal content on the ORR.



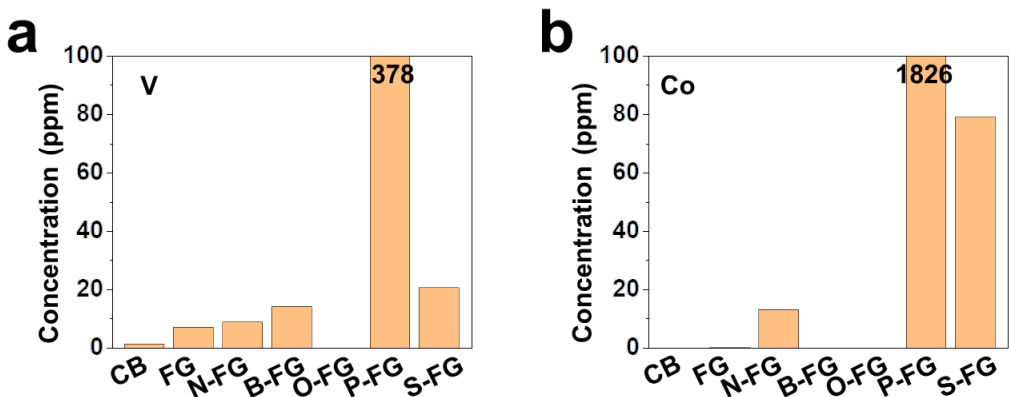
图S32。 通过ICP-MS测定杂原子掺杂FG中各种痕量金属的浓度。
Figure S32. The concentration of various trace metals in heteroatom-doped FG as determined by ICP-MS. These six different transition metals, Ir, Pd, Pt, Au, Ru, Mo, have been reported as effective catalysts or components.³² Ir, Pd, Pt, Au, and Ru cannot be detected or have a very low concentration (<1 ppm). The concentrations of Mo are 2~3 orders of magnitude lower than the concentrations reported in the previous literature.²⁹⁻³¹ In addition, there is no obvious relationship²⁹⁻³¹此外，没有明显的关系

在这些金属的浓度和杂原子掺杂FG的催化性能之间。

between the concentrations of these metals and the catalytic performance of the heteroatom-

这些发现表明，金属含量对ORR的影响最小。

doped FG. These findings suggest minimal effect of metal content on the ORR.



图S33。通过ICP-MS测定杂原子掺杂FG中各种痕量金属的浓度。

Figure S33. The concentration of various trace metals in heteroatom-doped FG as determined by

除P-FG外，这两种不同过渡金属(V和Co)的浓度较低。

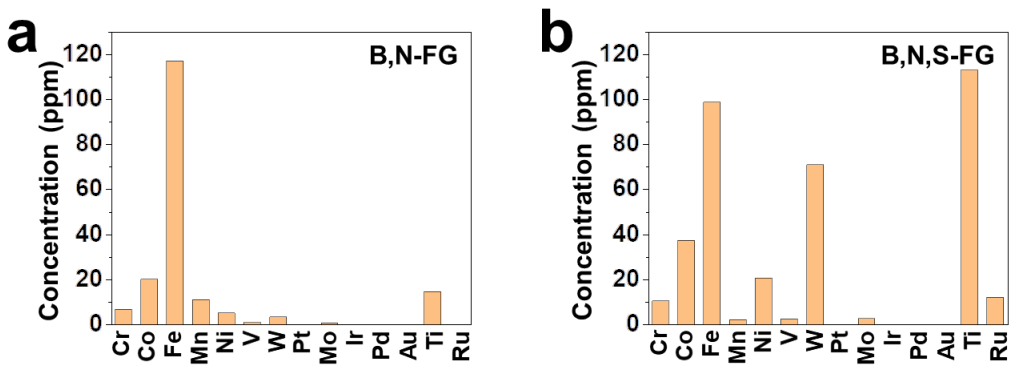
ICP-MS. The concentrations of these two different transition metals (V and Co) are low except

在P-FG产品中，V和Co的浓度分别为378 ppm和1826 ppm。

for P-FG. The concentration of V and Co are 378 ppm and 1826 ppm, respectively, in the P-FG

由于碳源和闪速反应本身不会导致这些金属的增加，P-FG中的金属含量来自红磷。
product. Since the carbon source, and the flash reaction itself will not cause the increase of these

metals, the metal content from P-FG is from the red phosphorus.



图S34。通过ICP-MS测定杂原子掺杂FG中各种痕量金属的浓度。

Figure S34. The concentration of various trace metals in heteroatom-doped FG as determined by ICP-MS. For the co-doped FG, in total 14 different types of the metals are tested. For the detectable metals, the concentrations of these metals are 1~4 orders of magnitude lower than the values reported in previous papers.²⁹⁻³¹ These findings suggest minimal effect of metal content on the ORR.

对于可检测的金属，这些金属的浓度比以前文献中报告的值低1~4个数量级。
对于共掺杂FG，共测试了14种不同类型的金属。

表S1。不同系统的电能。
Table S1. Electrical energy for different systems.

材料 Materials	电能(kJ g ⁻¹) Energy cost(美元/吨) ¹ Electrical energy (kJ g ⁻¹)	Energy cost (USD per ton) ¹
N-FG	6.6	36.8
B-FG	1.2	6.3
O-FG	1.5	8.1
F-FG	1.6	8.7
P-FG	8.1	45.0
S-FG	10.7	59.0
B,N-FG	3.5	19.6
B,N,S-FG	3.5	19.4
FG	7.2	40.0

¹: 能源成本是根据每千瓦时2美分的电价计算的，这是
¹: The energy cost is calculated based on the electricity price is 2 cents per kWh which is the
 西得克萨斯州工业税率。
 West Texas industrial rate.

表S2。N-FG样品反褶积N 1s谱的相对分布

Table S2. Relative distributions of deconvoluted N 1s spectra of N-FG samples

功能组 Functional groups	N-FG (%)	N-FG-L2 (%)
吡啶N Pyridinic N	46.6	41.3
吡咯氮 Pyrrolic N	42.7	44.7
石墨N Graphitic N	10.8	14.1

对于N-FG和N-FG-L2，吡啶氮和石墨氮的比率分别为4.31和2.93。

The ratios of pyridinic N and graphitic N are 4.31 and 2.93 for N-FG and N-FG-L2. These

啶氮原子具有未配对的电子自旋密度，并与某些物种(如金属原子)表现出强烈的相互作用，这在电催化剂或

pyridinic nitrogen atoms have unpaired electron spin density and exhibit strong interactions with

金属电沉积的潜在应用中非常有用。

some species, like metal atoms, which is useful in potential applications in electrocatalysts or

metal electrodeposition.

这些吡

啶氮原子具有未配对的电子自旋密度，并与某些物种(如金属原子)表现出强烈的相互作用，这在电催化剂或

pyridinic nitrogen atoms have unpaired electron spin density and exhibit strong interactions with

金属电沉积的潜在应用中非常有用。

some species, like metal atoms, which is useful in potential applications in electrocatalysts or

metal electrodeposition.

表S3。最近报道中掺杂石墨烯的石墨烯质量
Table S3. The graphene quality of doped graphene in recent reports

材料 Materials	方法 Methods	I _D /I _G	I _{2D} /I _G	参考 Reference
硼掺杂石墨烯 Boron doped graphene	电弧放电 Arc discharge	1.16	0.25	6
墨烯电弧放电 Nitrogen doped graphene	Arc discharge	1.03	0.62	6
墨烯热退火 Nitrogen doped graphene	Thermal annealing	1.67	n/a ⁷	7
墨烯 Boron doped graphene	热退火 Thermal annealing	1.66	n/a	7
Boron doped graphene	热退火 Thermal annealing	0.84	0.13	8
烯 Boron doped graphene	激光诱导合成 Laser-induced synthesis	0.67	0.60	9
Boron doped graphene	热退火 Thermal annealing	0.57	0.10	10
Boron doped graphene	热退火 Thermal annealing	0.54	n/a	11
Boron doped graphene	热退火 Thermal annealing	0.69	0.27	12
烯热退火 Nitrogen doped graphene	Thermal annealing	1.04	0	12
掺硼石墨烯 Boron doped graphene	热退火 Thermal annealing	0.93	0.10	13
Boron doped graphene	化学还原 Chemical reduction	1.16	0	14
掺硼石墨烯 Boron doped graphene	热退火 Thermal annealing	1.30	n/a	15
Boron doped graphene	热退火 Thermal annealing	1.10	n/a	15
烯热退火 Nitrogen doped graphene	Thermal annealing	0.96	0.14	16
烯化学还原 Fluorine doped graphene	Chemical reduction	0.87	0.08	17
烯化学还原 Fluorine doped graphene	Chemical reduction	1.31	0.20	17
Boron doped graphene	热反应 Thermal reaction	0.20	n/a	18
Boron doped graphene	化学气相沉积 Chemical vapor deposition	0.49	1.95	19
0.25硼掺杂石墨烯 Phosphorus doped graphene	Chemical vapor deposition	0.20	0.25	20
Boron doped graphene	化学气相沉积 Chemical vapor deposition	1.82	0.76	21

氮掺杂石墨烯热退火 Nitrogen doped graphene	Thermal annealing	0.81 0.81	0.08 0.08	22	氮掺杂石墨
烯等离子体处理 Nitrogen doped graphene	Plasma treatment	0.80 0.80	0.12 0.12	23	掺氟石墨烯
激光诱导合成 Fluorine doped graphene	Laser-induced synthesis	1.12 1.12	0.18 0.18	24	

¹: 不适用表示无法在论文中获得该值。
¹: n/a means the value can not be obtained in the papers.

为了证明I_{2D}/I_G=0.10可以作为基准的结论，参考了最近关于掺杂石墨烯的出版物。

To justify the conclusion that “I_{2D}/I_G=0.10” can be used here as the benchmark, recent publications on doped graphene are referenced. Since the heteroatom doping can cause the decrease of I_{2D} and increase of I_D, we list the Raman results of I_{2D} to I_G and I_D to I_G in Table S3

由于杂原子掺杂可以导致I_{2D}的减少和I_D的增加，我们在上面的表S3中列出了I_{2D}到IG和ID到IG的拉曼结果。
选择统计中值0.10作为阈值，以确定材料是否为石墨烯。

above. The statistical median 0.10 is chosen as the threshold value to determine if the material is graphene or not.

表S4。 杂原子掺杂FG的石墨烯质量。
Table S4. The graphene quality of heteroatom-doped FG.¹

材料 Materials	I _{2D} /I _G	I _D /I _G	石墨烯含量产率 Graphene content yield
CB	0.06	0.98	0
FG	1.95	<0.05	100%
B-FG	0.26	0.91	94%
N-FG	0.84	0.65	100%
O-FG	0.87	0.83	100%
F-FG ²⁵	0.26	0.65	94%
P-FG	0.17	0.85	86%
S-FG	0.24	0.76	88%
B,N-FG	0.32	0.90	89%
B,N,S-FG	0.85	0.83	87%
N-FG-L2 ²	0.44	1.08	99%

¹: 表S4中的统计数据是基于100个采样点而不是N-FG计算的-
¹: The statistical data in Table S4 are calculated based on 100 sampling points, other than N-FG-

L2.

²: N-FG-L2的统计数据基于200个采样点计算

²: The statistical data of N-FG-L2 are calculated based on 200 sampling points

表S5。 杂原子掺杂FG的晶体结构。
Table S5. The crystal structure of heteroatom-doped FG.

材料 Materials	(002)位置/度 (002) position/degree	层间距/Å Interlayer spacing/Å	平均尺寸/nm Average size/nm
CB	n/a	n/a	~12.0
FG	26.15	3.40 (+1.7%) ¹	16.0~27.0
CG	26.61	3.35	>100
B-FG	25.96	3.43 (+2.5%)	24.2
N-FG	25.89	3.44 (+2.7%)	98.9
O-FG	26.06	3.42 (+2.1%)	40.2
F-FG ²⁵	26.40	3.37 (+0.8%)	~25.0
P-FG	25.95	3.43 (+2.5%)	38.8
S-FG	26.42	3.37 (+0.7%)	42.5
B,N-FG	25.91	3.44 (+2.6%)	49.9
B,N,S-FG	26.01	3.42 (+2.2%)	76.0
N-FG-L2	26.04	3.42 (+2.1%)	41.2

: 括号()中的值显示了与AB堆叠石墨烯相比层间距的百分比变化，其中等式12用于计算百分比变化：
¹: The values in the parentheses (), show the percentage change of interlayer spacing compared

with AB-stacked graphene, where eq 12 is used to calculate the percentage change:

$$\text{Percentage Change} = \frac{\text{Interlayer spacing}_{\text{doped FG}} - \text{Interlayer spacing}_{\text{AB-stacked graphene}}}{\text{Interlayer spacing}_{\text{AB-stacked graphene}}} \times 100\% \quad (12)$$

表S6。研究了不同杂原子掺杂FG在0.1 M KOH溶液中的电化学氧还原性能。

Table S6. The electrochemical oxygen reduction performance of various heteroatom-doped FG

in 0.1 M KOH solution.

材料 Materials	过电位1/V Overpotential ¹ /V	塔菲尔斜率/mV dec ⁻¹ Tafel slope/mV dec ⁻¹
N-FG	0.75	54
B-FG	0.66	85
O-FG	0.57	75
S-FG	0.88	74
B,N-FG	0.75	58
CB	0.61	78
FG	0.53	83
Pt/C (20 wt% Pt) ²⁶	~0.96	~70

¹: 表中使用0.2 mA cm⁻²下的电位进行比较。

¹: The potentials at 0.2 mA cm⁻² are used for comparisons in the Table.

工具书类

References

1 Luong , D.X. ; 贝茨 , K.V. ; Algozeeb , W.A. ; 斯坦福 , M.G. ; Kittrell , C. ; 陈 , W. ; Salvatierra , R.V. ; 任 , M. ; 麦克休 , E.A. ; Advincula , P.A. ; 王 , Z. ; Bhatt , M. ; 郭 , H. ; 曼切夫斯 , Salvatierra, R. V.; Ren, M.; McHugh, E. A.; Advincula, P. A.; Wang, Z.; Bhatt, M.; Guo, 基 , V. ; Shahsavari , R. ; 雅各布森 , B.I. ; 图尔 , J.M. 克尺度自底向上闪光石墨烯合成。 H.; Mancevski, V.; Shahsavari, R.; Yakobson, B. I.; Tour, J. M. Gram-Scale Bottom-Up

《自然》2020 , 577647-651。

Flash Graphene Synthesis. *Nature* **2020**, 577, 647-651.

2 陈 , W. ; 王 , Z. ; 贝茨 , K.V. ; Luong , D.X. ; 任 , M. ; 斯坦福 , M.G. ; 麦克休 , E.A. ; Algozeeb , W.A. 。 ; 郭 , H. ; 高 , B. ; 邓 , B. ; 陈 , J. ; 季 , L. ; 卡斯滕 , W.T. ; 雅各布森 , B.I. ; Tour , J.M. 通过闪光 A.; Algozeeb, W. A.; Guo, H.; Gao, G.; Deng, B.; Chen, J.; Li, J. T.; Carsten, W. T.; 焦耳加热实现亚稳2D材料的毫秒转换。

Yakobson, B. I.; Tour, J. M. Millisecond Conversion of Metastable 2D Materials by

Flash Joule Heating. *ACS Nano* **2021**, 15, 1282-1290.

3 Algozeeb , W.A. ; 萨瓦斯 , P.E. ; Luong , D.X. ; 陈 , W. ; Kittrell , C. ; Bhat , M. ; Shahsavari , R. ; Tour , J.M. 从塑料废料中提取石墨烯。 R.; Tour, J. M. Flash Graphene from Plastic Waste. *ACS Nano* **2020**, 14, 15595-15604.

- 4 Nakanishi , K. 孔隙度测量。 溶胶-凝胶科学技术手册。
 4 Nakanishi, K. Porosity Measurement. Handbook of Sol-Gel Science and Technology.
 Springer International Publishing AG 2016 , 1-11。 内政部 : 10.1007/978-3-319-19454-7_38-
 Springer International Publishing AG 2016, 1-11. DOI: 10.1007/978-3-319-19454-7_38-
- 1.
- 5 Radlinski , A.P. ; Mastalerz , M. ; Hinde , A.L. ; Hainbuchner , M. ; Rauch , H. ; Baron , M. ; 林。
 5 Radlinski, A. P.; Mastalerz, M.; Hinde, A. L.; Hainbuchner, M.; Rauch, H.; Baron, M.;
 ; Fan , L. ; Thiagarajan , P. SAXS和SANS在评估煤的孔隙度、孔径分布和表面积中的应用。
 Lin, J. S.; Fan, L.; Thiagarajan, P. Application of SAXS and SANS in Evaluation of
 内景J. 煤岩土。
 Porosity, Pore Size Distribution and Surface Area of Coal. *Int. J. Coal Geol.* **2004**, 59,
 245-271.
- 6 Panchakarla , L.S. ; Subrahmanyam , K.S. ; 萨哈 , S.K. ; Govindaraj , A. ; Krishnamurthy , H.R. ;
 6 Panchakarla, L. S.; Subrahmanyam, K. S.; Saha, S. K.; Govindaraj, A.; Krishnamurthy,
 Waghmare , U.V. ; Rao , C.N.R. 硼和氮掺杂石墨烯的合成、结构和性能。
 H. R.; Waghmare, U. V.; Rao, C. N. R. Synthesis, Structure, and Properties of Boron-
 高级材料。
 and Nitrogen-Doped Graphene. *Adv. Mater.*, **2009**, 21, 4726-4730.
- 7 亩 , X. ; 袁 , B. ; 冯 , X. ; 邱 , 宋 , L. ; 胡 , Y. 掺杂杂原子(氮、硼、磷)对还原氧
 7 Mu, X.; Yuan, B.; Feng, X.; Qiu, S.; Song, L.; Hu, Y. The Effect of Doped Heteroatoms
 化石墨烯热氧化的抑制作用。
 (Nitrogen, Boron, Phosphorus) On Inhibition Thermal Oxidation of Reduced Graphene
 Oxide. *RSC Adv.*, **2016**, 6, 105021-105029.
- 8 Sheng , Z.-H. ; 高 , H-L. ; 鲍 , F-B. ; 夏 , X-H. 燃料电池氧还原反应用掺硼石墨烯的合成。
 8 Sheng, Z. -H.; Gao, H. -L.; Bao, W. -J.; Wang, F. -B.; Xia, X. -H. Synthesis of Boron
 J. 马特。 化学。 , 2012,
 Doped Graphene for Oxygen Reduction Reaction in Fuel Cells. *J. Mater. Chem.*, **2012**,
 22, 390-395.
 22, 390-395.
- 9 彭 , Z. ; Ye , R. ; Mann , J.A. ; Zakhidov , D. ; 李 , Y. ; 斯莫利 , P.R. ; 林 , J. ; Tour , J.M. 柔性掺硼
 9 Peng, Z.; Ye, R.; Mann, J. A.; Zakhidov, D.; Li, Y.; Smalley, P. R.; Lin, J.; Tour, J. M.
 激光诱导石墨烯微超级电容器。
 Flexible Boron-Doped Laser-Induced Graphene Microsupercapacitors. *ACS Nano* **2015**,
 9, 5868-5875.
- 10 Vineesh , T.V. ; Kumar , M.P. ; 高桥 , C. ; Kalita , G. ; Alwarappan , S. ; Pattanayak , D.K. ;
 10 Vineesh, T. V.; Kumar, M. P.; Takahashi, C.; Kalita, G.; Alwarappan, S.; Pattanayak, D.
 Narayanan , T.N. 碳化硼衍生的掺硼石墨烯的双功能电催化活性。
 K.; Narayanan, T. N. Bifunctional Electrocatalytic Activity of Boron-Doped Graphene
 高级能源材料。
 Derived from Boron Carbide. *Adv. Energy Mater.* **2015**, 5, 1500658.

- 11 Khai , T.V。 ; Na , H.G。 ; Kwak , D.S。 ; Kwon , Y.J。 ; Ham , H。 ; 垫片 , K.B。 ; 金 , H.W。 掺硼和未掺硼
 11 Khai, T. V.; Na, H. G.; Kwak, D. S.; Kwon, Y. J.; Ham, H.; Shim, K. B.; Kim, H. W.
 氧化石墨烯薄膜结构和光学性能的比较研究。
 Comparison Study of Structural and Optical Properties of Boron-Doped and Undoped
 化学。工程。
 Graphene Oxide Films. *Chem. Eng. J.*, **2012**, 211, 369-377.
- 12 田 , H。 ; 王。 ; Sofer , Z。 ; Pumera , M。 ; Bonanni , A.掺杂石墨烯用于DNA
 12 Tian, H.; Wang, L.; Sofer, Z.; Pumera, M.; Bonanni, A. Doped Graphene for DNA
 分析：电化学信号受到掺杂剂种类和碱基结构的强烈影响。
 Analysis: The Electrochemical Signal is Strongly Influenced by the Kind of Dopant and
 the Nucleobase Structure. *Sci. Rep.*, **2016**, 6, 33046.
- 13 Yeom , D-Y。 ; Jeon , W。 ; 屠。 ; Yeo , S.Y。 ; Lee , S-S。 ; 宋 , B.J。 ; 张 , H。 ; Lim , J.A。 ; Kim , H。
 13 Yeom, D. -Y.; Jeon, W.; Tu, N. D. K.; Yeo, S. Y.; Lee, S. -S.; Sung, B. J.; Chang, H.;
 通过简单热退火的石墨烯纳米片的高浓度硼掺杂及其超级电容特性。
 Lim, J. A.; Kim, H. High-Concentration Boron Doping of Graphene Nanoplatelets By
 Simple Thermal Annealing and Their Supercapacitive Properties. *Sci. Rep.*, **2015**, 5,
 09817.
- 14 Sahoo , M。 ; Sreena , K.P。 ; Vinayan , B.P。 ; Ramaprabhu , S.掺硼石墨烯的绿色合成及其作为锂离子电
 14 Sahoo, M.; Sreena, K. P.; Vinayan, B. P.; Ramaprabhu, S. Green Synthesis of Boron
 池高性能阳极材料的应用。
 Doped Graphene and Its Application as High Performance Anode Material in Li Ion
 马特。 Bull研究。
 Battery. *Mater. Res. Bull.*, **2015**, 61, 383-390.
- 15 余 , X。 ; 韩 , P。 ; 魏 , Z。 ; 黄。 ; 顾 , Z。 ; 彭。 ; 马 , J。 ; 郑 , G。 用于电催化N2还原的掺硼石墨烯。
 15 Yu, X.; Han, P.; Wei, Z.; Huang, L.; Gu, Z.; Peng, S.; Ma, J.; Zheng, G. Boron-Doped
 焦耳 , 2018 , 2 , 1610-1622。
 Graphene for Electrocatalytic N₂ Reduction. *Joule*, **2018**, 2, 1610-1622.
- 16 Iglesias , D。 ; 朱利安尼 , A。 ; Melchionna , M。 ; Marchesan , S。 ; Criado , A。 ; Nasi , L。 ;
 16 Iglesias, D.; Giuliani, A.; Melchionna, M.; Marchesan, S.; Criado, A.; Nasi, L.;
 Bevilacqua , M。 ; 塔瓦格纳科 , C。 ; 维扎 , F。 ; Prato , M。 ; Fornasiero , P.N掺杂石墨化碳纳米角
 Bevilacqua, M.; Tavagnacco, C.; Vizza, F.; Prato, M.; Fornasiero, P. N-Doped
 作为高选择性O₂还原为H₂O₂的前沿电催化剂。化学 , 2018 , 40106-123。
 Graphitized Carbon Nanohorns as a Forefront Electrocatalyst in Highly Selective O₂
 Reduction to H₂O₂. *Chem*, **2018**, 4, 106-123.
- 17 奈尔 , R.R。 ; 任。 ; Jalil , R。 ; Riaz , I。 ; Kravets , V.G。 ; Britnell , L。 ; 布莱克 , P。 ; Schedin , F
 17 Nair, R. R.; Ren, W.; Jalil, R.; Riaz, I.; Kravets, V. G.; Britnell, L.; Blake, P.; Schedin,
 。 ; 马约罗夫。 ; 袁。 ; Katsnelson , M.I。 ; 程 , H-M。 ; 斯特鲁平斯基 , W。 ; Bulusheva , L.G。 ;
 F.; Mayorov, A. S.; Yuan, S.; Katsnelson, M. I.; Cheng, H. -M.; Strupinski, W.;
 Okotrub , A.V。 ; Grigorieva , I.V。 ; 格里戈连科。 ; 诺沃塞洛夫 , K。
 Bulusheva, L. G.; Okotrub, A. V.; Grigorieva, I. V.; Grigorenko, A. N.; Novoselov, K.

S盖姆 , A.K. 荧光石墨烯 : 聚四氟乙烯的二维对应物。
S.; Geim, A. K. Fluorographene: A Two-Dimensional Counterpart of Teflon. *Small*,
2010, 6, 2877-2884.

18 Kim , Y.A. ; 藤泽 , K. ; 村松 , H. ; 林 , T. ; Endo , M. ; 藤森。 ; K.Kaneko。 ; Terrones , M. ;
18 Kim, Y. A.; Fujisawa, K.; Muramatsu, H.; Hayashi, T.; Endo, M.; Fujimori, T.; Kaneko,
Behrends , J. ; 埃克曼 , A. ; Casiraghi , C. ; Novoselov , K.S. ; Saito , R. ; Dresselhaus ,
K.; Terrones, M.; Behrends, J.; Eckmann, A.; Casiraghi, C.; Novoselov, K. S.; Saito, R.;
M.S.ACS Nano 2012 , 66293-6300.
Dresselhaus, M. S. *ACS Nano* **2012**, 6, 6293-6300.

19 李 , X. ; Fan , L. ; 李 , Z. ; 王 , K. ; 钟 , M. ; 魏 , J. ; 吴 , D. ; 朱 , H. 石墨烯-硅p-n结太阳能电池
19 Li, X.; Fan, L.; Li, Z.; Wang, K.; Zhong, M.; Wei, J.; Wu, D.; Zhu, H. Boron Doping of
中石墨烯的硼掺杂。
Graphene for Graphene-Silicon p-n Junction Solar Cells. *Adv. Energy Mater.*, **2012**, 2,

425-429.

20 Ovezmyradov , M. ; Magedov , I.V. ; Frolova , L.V. ; 钱德勒 , G. ; 加西亚 , J. ; Bethke , D. ;
Ovezmyradov, M.; Magedov, I. V.; Frolova, L. V.; Chandler, G.; Garcia, J.; Bethke, D.;
Shaner , E.A. ; Kalugin , N.G. 使用含苯基分子的磷和硼掺杂石墨烯的化学气相沉积。
Shaner, E. A.; Kalugin, N. G. Chemical Vapor Deposition of Phosphorous- and Boron-

Doped Graphene Using Phenyl-Containing Molecules. *J. Nanosci. Nanotechnol.*, **2015**,
15, 4883-4886.

21 王。 ; 周 , Y. ; 吴博士。 ; 廖。 ; 赵。 ; 彭 , H. ; 刘 , Z. 使用唯一的固体原料通过化学气相沉积合成硼掺
21 Wang, H.; Zhou, Y.; Wu, D.; Liao, L.; Zhao, S.; Peng, H.; Liu, Z. Synthesis of Boron-
杂石墨烯单分子膜。
Doped Graphene Monolayers Using the Sole Solid Feedstock by Chemical Vapor

Deposition. *Small* **2013**, 9, 1316-1320.

22 Sheng , Z.-H. ; 邵。 ; 陈。 ; 鲍。 ; 王 , F-B. ; 夏 , X-H. 通过三聚氰胺热退火氧化石墨制备氮掺杂石墨
22 Sheng, Z. -H.; Shao, L.; Chen, J. -J.; Bao, W. -J.; Wang, F. -B.; Xia, X. -H. Catalyst-Free
烯及其优异的电催化性能。
Synthesis of Nitrogen-Doped Graphene via Thermal Annealing Graphite Oxide with

Melamine and Its Excellent Electrocatalysis. *ACS Nano* **2011**, 5, 4350-4358.

23 Rybin , M. ; Pereyaslavtsev , A. ; 瓦西里耶娃 , T. ; 迈亚斯尼科夫。 ; Sokolov , I. ; 巴甫洛娃 , A.
23 Rybin, M.; Pereyaslavtsev, A.; Vasilieva, T.; Myasnikov, V.; Sokolov, I.; Pavlova, A.;
; Obraztsova , E. ; 霍米奇 , A. ; 拉尔琴科 , V. ; Obraztsova , E. 等离子体处理石墨烯的高效氮掺
Obraztsova, E.; Khomich, A.; Ralchenko, V.; Obraztsova, E. Efficient Nitrogen Doping
杂。
of Graphene by Plasma Treatment. *Carbon* **2016**, 96, 196-202.

- 24 Ye, R.; 韩, X.; Kosynkin, D. V.; 李, Y.; 张, C.; 姜, B.; Marti, A. A.; 激光诱导聚四氟乙烯
24 Ye, R.; Han, X.; Kosynkin, D. V.; Li, Y.; Zhang, C.; Jiang, B.; Marti, A. A.; Tour, J. M.
转化为氟化纳米金刚石或氟化石墨烯。
Laser-Induced Conversion of Teflon into Fluorinated Nanodiamonds or Fluorinated
Graphene. *ACS Nano* **2018**, 12, 1083-1088.
- 25 陈, W.; 李, Z.; Algozeeb, W. A.; Luong, D. X.; Kittrell, C.; 麦克休, E. A.; Advincula,
25 Chen, W.; Li, J. T.; Wang, Z.; Algozeeb, W. A.; Luong, D. X.; Kittrell, C.; McHugh, E.
P. A.; Wyss, K. M.; 贝克汉姆, J. L.; 斯坦福, M. G.; 姜, B.; Tour, J. M.;
A.; Advincula, P. A.; Wyss, K. M.; Beckham, J. L.; Stanford, M. G.; Jiang, B.; Tour, J. M.
闪光焦耳加热的超快可控相变演化。
Ultrafast and Controllable Phase Evolution by Flash Joule Heating. *ACS Nano* **2021**, 15,
11158-11167.
- 26 陈, ; 季, ; 赵, ; 陈, W.; 董, J.; Cheong, W.-C.; 沈, R.; 温, X.; 郑, ; Rykov, A. I.; 蔡, ;
26 Chen, Y.; Ji, S.; Zhao, S.; Chen, W.; Dong, J.; Cheong, W. -C.; Shen, R.; Wen, X.; Zheng,
唐, H.; 庄, Z.; 陈, ; 彭, ; 王, D.; 李, Y. 锌-空气电池和氢-空气燃料电池的单原子位铁催化
L.; Rykov, A. I.; Cai, S.; Tang, H.; Zhuang, Z.; Chen, C.; Peng, Q.; Wang, D.; Li, Y.
剂增强氧还原。
Enhanced Oxygen Reduction with Single-Atomic-Site Iron Catalysts for a Zinc-Air
电池 and Hydrogen-Air Fuel Cell. *Nat. Commun.*, **2018**, 9, 5422.
- 27 王, ; 李, ; 张, C.; 程, Z.; 陈, W.; 麦克休, E. A.; 卡特, R. A.; 雅各布森, B. I.; Tour, J. M. 无
27 Wang, Z.; Li, Q. -K.; Zhang, C.; Cheng, Z.; Chen, W.; McHugh, E. A.; Carter, R. A.;
金属炭黑上100%法拉第效率的过氧化氢生成。
Yakobson, B. I.; Tour, J. M. Hydrogen Peroxide Generation with 100% Faradaic
ACS加泰罗尼亚。
Efficiency on Metal-Free Carbon Black. *ACS Catal.*, **2021**, 11, 2454-2459.
- 28 邓, B.; Luong, D. X.; 王, Z.; Kittrell, C.; 麦克休E.A.; Tour, J.M. 闪光焦耳加热城市采矿。
28 Deng, B.; Luong, D. X.; Wang, Z.; Kittrell, C.; McHugh E. A.; Tour, J. M. Urban Mining
纳特。
by Flash Joule Heating. *Nat. Commun.* **2021**, 12, 5794.
- 29 王, ; Sofer, Z.; Pumera, M. 我们在石墨烯中添加的垃圾会增加其电催化效果吗?
29 Wang, L.; Sofer, Z.; Pumera, M. Will Any Crap We Put into Graphene Increase Its
Electrocatalytic Effect? *ACS Nano* **2020**, 14, 21-25.
- 30 Ye, R.; 董, J.; 王, ; 克鲁兹, R. M.; 李, Y.; 安, P.-F.; 亚卡曼, M. J.; 雅各布森, B.
30 Ye, R.; Dong, J.; Wang, L.; Cruz, R. M.; Li, Y.; An, P. -F.; Yacaman. M. J.; Yakobson, B.
B. I.; 陈, D.; Tour, J. M. 锰对石墨烯的欺骗及其在催化中的意义。
I.; Chen, D.; Tour, J. M. Manganese Deception on Graphene and Implications in
碳2018, 132, 623-631。
Catalysis. *Carbon* **2018**, 132, 623-631.

31 王。 ; 安布罗西 , A. ; Pumera , M. 掺杂杂原子的石墨烯上的无金属催化氧还原反应是由微量金属杂质引起的
31 Wang, L.; Ambrosi, A.; Pumera, M. “Metal-Free” Catalytic Oxygen Reduction Reaction

。 安吉。 化学。 内景。
on Heteroatom-Doped Graphene is Caused by Trace Metal Impurities. *Angew. Chem. Int.*

Ed. **2013**, 52, 13818-13821.

32 夏 , W. ; Mahmood , A. ; 梁。 ; 邹 , R. ; 郭。 用于氧还原的地球丰富的纳米材料。

32 Xia, W.; Mahmood, A.; Liang, Z.; Zou, R.; Guo, S. Earth-Abundant Nanomaterials for
Oxygen Reduction. *Angew. Chem. Int. Ed.* **2016**, 55, 2650-2676.